ISSN No. 2454-6194 | DOI: 10.51584/IJRIAS |Volume VIII Issue XII December 2023

Analytical and Numerical Solutions for Heat, Mass and Entropy Generation of Fourth Grade Nanofluid Flow over a Vertical Plate

***Aroloye, Soluade Joseph, Fenuga Olugbenga John, Abiala Israel Olatunji and Okunuga Solomon Adewale**

Department of Mathematics, Faculty of Science, University of Lagos, Nigeria.
**Corresponding Author*
DOI: https://doi.org/10.51584/IJRIAS.2023.81213

Received: 16 November 2023; Revised: 06 December 2023; Accepted: 09 December 2023; Published: 06 January 2024

Abstract: The focus of this research is to investigate magnetohydrodynamic flow, entropy generation, heat and mass transfer analysis for fourth grade nanofluid over a vertical plate in a porous medium subject to slip and convective boundary conditions. Lie group invariant similarity variable is used to transform the partial differential equations (PDEs) governing the problem to system of coupled nonlinear ordinary differential equations (ODEs). The resulting dimensionless ODEs are solved using Homotopy Perturbation Method (HPM). HPM results are validated with the numerical solutions via shooting method alongside the six order Runge-Kutta integration technique. The results revealed effects of new embedded governing flow parameters on velocity, temperature, entropy generation and concentration profiles. Furthermore, the impact of new embedded flow parameters on skin friction coefficient, Nusselt number and Sherwood number at the plate surface are investigated and the results are shown in tabular forms. The results indicate that suction on the plate can be used to control momentum, thermal and solutal boundary layer thickness. This research discovered that magnetic parameter, Eckert number, Biotsolutal number and Hartmann number can be respectively used to adjust fluid flow's velocity, temperature, concentration and entropy generation. This research also detected that the force driving the fourth grade nanofluid flow called buoyancy driven force can be accelerated or decelerated by adjusting angle of magnetic field inclination. The present investigation has applications in industries and engineering, such as petroleum industries, chemical industries and metallurgy sciences

Keywords: Entropy generation, Fourth grade nanofluid, Heat and mass transfer, Homotopy Perturbation Method (HPM), Unsteady magnetohydrodynamic (MHD) flow.

I. Introduction

It is well known that convectional Newtonian/ non-Newtonian fluids have poor heat transfer performance, due to low thermal conductivity. To improve the thermal conductivity of these fluids, nano-or micro-sized particles are suspended (Khan et al., 2015). Choi and Eastman (1995) first introduced and used the word 'nanofluid', which is a mixture of nanoparticles and base fluids (Newtonian/non-Newtonian). These nanofluids significantly increase heat transfer rates in several areas, such as industrial reactors, transportation industry, micro-electromechanical systems and biomedical applications. Choiet al., (2001) showed that the addition of a small amount (less than 1% by volume) of nanoparticles to convectional heat transfer liquids increased the thermal conductivity of the fluid by up to approximately two times. Comprehensive analyses of convective transport in nanofluids were made by Buonigiorno (2006).Tarun et al., investigate the analysis of entropy generation due to MHD natural convective flow in an Inclined channel in the presence of magnetic field and Heat Source Effects. Hayat et al.,(2002) presented flow of a fourth grade fluid. They watered down the problem by assuming steady flow while solving the governing equation governing the flow.Tarun et al. (2023) examined the hemical reactive magnetized fluid flow through a vertical channel due to heat source and thermal radiation effects. Nadeem et al.,(2010) took analytical approach to study the problem of effects of partial slip on a fourth grade fluid with variable viscosity. Pooja et al., investigated (2016) Entropy Analysis in MHD Forced Convective Flow through a Circular Channel Filled with Porous Medium in the Presence of Thermal Radiation. Shah et al., (2010) examined Coutte and Poiseuille flows for fourth grade fluids. The nonlinear differential equation describing the velocity field was solved using optimal homotopy asymptotic method (OHAM). Hayatet al., (2011) presented the flow of a fourth-grade fluid with heat transfer. HAM was applied to solve the resulting boundary value problem. The optimal solution for the flow of a fourth–grade fluid with partial slip was investigated by Islam et al., (2011). Pooja et al., (2020) investigated entropy generation analysis of MHD forced convective flow through a horizontal porous channel. Aziz and Mahomed (2012) provided close form solutions for a nonlinear partial differential equation arising in the study of a fourth grade fluid model. Reduction and solutions for the unsteady flow of a fourth grade fluid on a porous plate was studied numerically and analytically by Aziz and Mahomed (2013). Tarun et al., (2023) investigated thermodynamical study of chemically-reactive and thermal-radiative magnetized oscillatory Couette flow in a porous medium filled channelSahood and Poncet (2013) numerically studied the problem of Blasium flow and h eat transfer of fourth grade fluid with slip. The investigation was limited to steady flow. Aziz et al., (2014) provided wave travelli ng solutions (both forward and backward type) for the unsteady MHD flow of a fourth grade fluid induced due to the impulsive motion of a flat porous plate. Tarun et al., (2021) examined the entropy generation in thermal radiative oscillatory MHD couette flow in the influence of heat source. Zaman et al., (2014) studied the problem of Stokes first problem for an unsteady MHD fourth

ISSN No. 2454-6194 | DOI: 10.51584/IJRIAS |Volume VIII Issue XII December 2023

–grade fluid in a non-porous half space with Hall currents. The problem of boundary layer flow of third grade nanofluid with Newtonian heating and viscous dissipation was investigated by Shehzad et al., (2015). Khan et al.,(2015) studied the combined heat and mass transfer of third grade nanofluids over a convectively- heated vertical plate. They found that the layer of nanofluid has many properties that different from the clear fluid. On modified algorithm for fourth-grade fluid was presented by Awan, et al., (2015). Rational homoptopy perturbation method (RHPM) was used to solve the problem. They failed to consider the heat and mass transfer aspect of the flow. Results on hydromagnetic flow of third grade nanofluid with viscous dissipation and flux condition was made available by Hussain et al.,(2015). Tarun et el., (2022) investigated the Study of dissipative MHD oscillatory unsteady free convective flow in a vertical channel occupied with the porous material in the presence of heat source effect and thermal radiation. Yurusoy (2016) applied perturbation method to investigate new analytical solutions for the flow of a fourth grade fluid past a porous plate. He ignored magnetic field and Darcy's resistance effect on the flow. Tarun et al.,(2023) investigated the analysis of second law of thermodynamics in unsteady magnetohydrodynamic buoyancy induced flow with heat source and thermal radiation. Bougoffa et al.,(2016) applied modified Adomian decomposition method (ADM) to present the exact and approximate analytic solutions of the thin film flow of fourth grade fluids. Carim et al.,(2 016) used a group theoretical analysis to examine unsteadymagentohydrodynamic flow of a fourth grade fluid caused by an impulsively moving plate in a Darcy porous medium. Aroloye et al., (2017) presented magnetohydrodynamic flow model of a fourth grade fluid in a porous medium. They found that suction on the plate can be used to control boundary layer thickness.

It can be seen from literature survey that researchers examine fourth grade fluid model to some limited extent and failed to look into fourth grade nanofluid model despite its industrial, science and engineering applications. It is obvious from literature survey that research on fourth grade nanofluid over a plate has not yet be reported. Previous studies on fourth grade fluid were carried out in the absent of nanofluid. Most of the above reviews on fourth grade fluid have been limited to steady flow, no slip, no temperature jump, no inclined magnetic field, absence of unsteady flow of heat and mass transfer analysis, no entropy generation, absence of nano particles concentration, no analysis of coefficient of skin friction, absence of nanofluid, no Darcy's resistance, no buoyancy driving force, no temperature and concentration distributions of unsteady flow. Motivated by the aforementioned, it is necessary to address these issues and bridge the gaps noticed in literature between fourth grade fluid and fourth grade nanofluid.

So, this research work focus on investigation of MHD flow, entropy generation, heat and mass transfer analysis for fourth grade nanofluid over a vertical plate in a porous medium subject to slip and convective boundary conditions. This research derived a semianalyticalapproach through Homotopy Perturbation Method (HPM) to solve the formulated differential equations governing the fourth grade nanofluid flow in terms of flow velocity, temperature, entropy gener ation and concen-tration fields. It established that the momentum, thermal and solutal boundary layer thickness of fourth grade nanofluid can be controlled/adjusted by suction velocity on the plate. Also, the buoyancy force which driven the fluid flow can be controlled by adjusting the angle of inclination of the magnetic field.

II. Mathematical Formulation of the problem

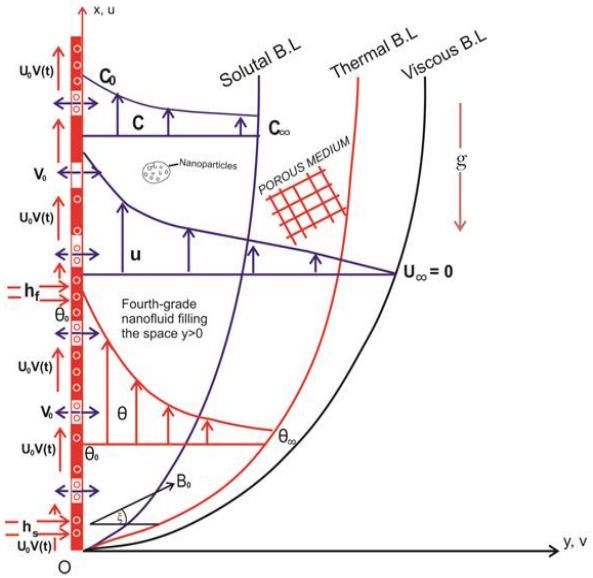

Figure 1: Geometry of the physical model and coordinate system (Fourth Grade Nanofluid)

Base on the nature of the problem considered, the appropriate modified continuity, momentum, heat and mass transfer equations of an electrically conducting, viscous, incompressible, chemically reacting fourth grade nanofluid in a porous medium under Boussinesq and Rosseland approximation, are given by

ISSN No. 2454-6194 | DOI: 10.51584/IJRIAS |Volume VIII Issue XII December 2023

Continuity equation $\nabla.\mathbf{V} = 0$ (1)

Momentum equation: $\rho_f \frac{d\mathbf{V}}{dt} = \nabla.\mathbf{T} + \mathbf{J}\ \mathrm{X}\ \mathbf{B} + \mathbf{R} + \rho_f \mathbf{g}\beta_T(\theta - \theta_\infty) + \rho_f \mathbf{g}B_c(C - C_\infty)$ (2)

Energy Equation: $\frac{d\theta}{dt} = \frac{k_f}{(\rho C_p)_f}\nabla^2\theta + \frac{1}{(\rho C_p)_f}tr(T.\nabla V) - \frac{1}{(\rho C_p)_f}\nabla.q_r + \frac{Q_0}{(\rho C_p)_f}(\theta - \theta_\infty) + \frac{\mu}{(\rho C_p)_f}|\nabla V|^2 + \tau\left[D_B\nabla C.\nabla\theta + \frac{D_r}{\theta_\infty}\nabla\theta.\nabla\theta\right],$ (3)

Mass Equation: $\frac{dC}{dt} = D_B\nabla^2 C + \frac{D_m k_T}{\theta_\infty}\nabla^2\theta - Kr(C - C_\infty).$ (4)

Where k_T is the thermal diffusion ratio, D_B is the Brownian diffusion coefficient, D_T is the thermophoresis diffusion coefficient, Q_0 is the internal heat generation, × denotes the vector product, K_r is the constant rate of chemical reaction, T is the Cauchy stress tensor for an incompressible fourth grade fluid, J is the current density, $\tau = \frac{(\rho C_p)_p}{(\rho C_p)_f}$ is the ratio between the effective heat capacity of the nanoparticle material and heat capacity of the fluid with ρ being the density, C_p is the specific heat capacity at constant pressure, β_C is the coefficient of concentration expansion, β_T is the coefficient of thermal expansion, g is the acceleration due to gravity, θ_0 wall temperature, θ_∞ ambient fluid temperature, B is the magnetic induction inclined at angle ξ the plate and **R** is the Darcy's resistance due to the porous medium, μ_f , is the dynamic viscosity of the base fluid, ρ_f is the base fluid density, k_f is the thermal conductivity, $(\rho c_p)_p$ is the effective heat capacity of the nanofluids particles and $(\rho c_p)_f$ is the effective heat capacity of the fluid. According to (Ramzan, Bila, Farooq and Chung, 2016), the radiative heat flux q_r , in equation (3) is described by Rosseland approximation for radiation as $\frac{\partial q_r}{\partial y} = -\frac{16\sigma^*\theta_\infty^3}{3k^*}\frac{\partial^2\theta}{\partial y^2}.$,where σ^* and k^* are the Stefan-Boltzmann constant and Rosseland mean absorption coefficient respectively. For the flow model under investigation, we seek a velocity field **V** temperature field, θ and Concentration fields C, respectively define as

$$\mathbf{V} = (u(y,t),-V_0,0,), \qquad \theta = \theta(y,t), \qquad C = C(y,t) \tag{5}$$

The velocity field in equation (5) identically satisfies the continuity equation (1). Thus, the disturbance in the fluid is a function of y and t only. Where $u(y,t)$ represents the fluid velocity, $V_0 > 0$ is the suction fluid velocity and $V_o < 0$ correspond to the injection fluid velocity. Since the fluid is electrically conducting for smallReynold s number and induced magnetic field is neglected. Following (Dada and Salawu, 2017), uniform magnetic strength B_0 is inclined to the plate at angle $0 < \xi < \frac{\pi}{2}$, can be expressed as $J \times B = -\sigma(\sin^2\xi)B_0^2 V$ (6)

The Cauchy stress tensor for a fourth grade fluid satisfies the constitutive equation (Aziz *et al.*, 2014) is

$$T = -I + \mu fA_1 + \alpha_1 A_2 + \alpha_2 A_1^2 + \beta_1 A_3 + \beta_2(A_2A_1 + A_1A_2) + \beta_3(trA_1^2)A_1 + \gamma_2(A_3A_1 + A_1A_3) + \gamma_1 A_4 + \gamma_3 A_2^2 + \gamma_4(A_2A_1^2A_2) + \gamma_5(trA_2)A_2 + \gamma_6(trA_2)A_1^2 + [\gamma_7(trA_3) + \gamma_8(trA_2A_1)]A_1 \tag{7}$$

ISSN No. 2454-6194 | DOI: 10.51584/IJRIAS |Volume VIII Issue XII December 2023

where P is the pressure, I is the identity matrix, μ_f is the base fluid viscosity, α_1 and α_2 are the second grade fluid parameters. β_1, β_2 and β_3 are the third grade fluid parameters and $\gamma_1, \gamma_2, \gamma_3, \gamma_4, \gamma_5, \gamma_6, \gamma_7$ and γ_8 are the fourth grade fluid parameters, A_1, A_2, A_3 and A_4 are Rivlin- Ericksen tensors. The tensors are defined as $A_1 = (\nabla V) + (\nabla V)^T$, $A_n = \frac{dA_{n-1}}{dt} + A_{n-1}(\nabla V) + (\nabla V)^T A_{n-1}, \quad for\ n > 1$ (8)

In which ∇ is the gradient operator, where T denotes the transpose of the resultant matrix. For the model (7), when $\alpha_i = 0, \beta_i = 0$, and $\gamma_i = 0$ the fluid is Newtonian, $\alpha_i \neq 0, \beta_i = 0$, and $\gamma_i = 0$ equivalent to second grade fluid $\alpha_i \neq 0, \beta_i \neq 0, \gamma_i = 0$, equivalent to the third grade fluid, $\alpha_i \neq 0, \beta_i \neq 0,$ and $\gamma_i \neq 0$, equivalent to fourth grade fluid. Substituting equations (5) - (8) into equations (1) - (4). Then, equations (3)-(4) respectively give the dimensional governing couple partial differential equations (PDEs) in u, θ and C as follows

$$\rho_f\left(\frac{\partial u}{\partial t} - V_0\frac{\partial u}{\partial y}\right) = \mu_f\frac{\partial^2 u}{\partial y^2} + \alpha_1\left(\frac{\partial^3 u}{\partial y^2\partial t} - V_0\frac{\partial^3 u}{\partial y^3}\right) + \beta_1\left(\frac{\partial^4 u}{\partial y^2\partial t^2} - 2V_0\frac{\partial^4 u}{\partial y^2\partial t} + V_0^2\frac{\partial^4 u}{\partial y^4}\right) +$$
$$6(\beta_2+\beta_3)\left(\frac{\partial u}{\partial y}\right)^2\frac{\partial^2 u}{\partial y^2} + \gamma_1\left(\frac{\partial^5 u}{\partial y^2\partial t^3} - 3V_0\frac{\partial^5 u}{\partial y^3\partial t^2} + 3V_0^2\frac{\partial^5 u}{\partial y^4\partial t} - V_0^3\frac{\partial^5 u}{\partial y^5}\right) + \rho f g\beta_C(C - C_\infty) +$$
$$2(3\gamma_2+\gamma_3+\gamma_4+\gamma_5+3\gamma_7+\gamma_8)\frac{\partial}{\partial y}\left|\left(\frac{\partial u}{\partial y}\right)^2\frac{\partial u}{\partial y\partial t} - V_0\left(\frac{\partial u}{\partial y}\right)^2\frac{\partial^2 u}{\partial y^2}\right| - \sigma f B_0^2(\sin^2\xi)u + \rho_f g\beta_T(0 - \theta_\infty)$$
$$-\frac{\phi}{\kappa}\begin{pmatrix} +\alpha_1\left(\frac{\partial u}{\partial y} - V_0\frac{\partial u}{\partial y}\right) + \beta_1\left(\frac{\partial^2 u}{\partial t^2} - 2V_0\frac{\partial^2 u}{\partial y\partial t} + V_0^2\frac{\partial^2 u}{\partial y^2}\right) \\ +2(\beta_2+\beta_3)u\left(\frac{\partial u}{\partial y}\right)^2 + \gamma_1\left(\frac{\partial^3 u}{\partial t^3} - 3V_0\frac{\partial^3 u}{\partial y\partial t^2} + 3V_0^2\frac{\partial^3 u}{\partial y^2\partial t} - V_0^3\frac{\partial^3 u}{\partial y^3}\right) + \mu_f u \\ +2(3\gamma_2+\gamma_3+\gamma_4+\gamma_5+3\gamma_7+\gamma_8)u\left(\frac{\partial u}{\partial y}\right)\left[\frac{\partial^2 u}{\partial y\partial t} - V_0\left(\frac{\partial^2 u}{\partial y^2}\right)\right] \end{pmatrix} \quad (9)$$

$$\left(\frac{\partial\theta}{\partial t} - V_0\frac{\partial\theta}{\partial y}\right) = \alpha_f\frac{\partial^2\theta}{\partial y^2} +$$
$$\frac{1}{(\rho c_P)_f}\begin{pmatrix} \mu\frac{\partial u}{\partial y} + \alpha_1\left(\frac{\partial^2 u}{\partial y\partial t} - V_0\frac{\partial^2 u}{\partial y^2}\right) + \beta_1\left(\frac{\partial^3 u}{\partial y\partial t^2} - 2V_0\frac{\partial^2 u}{\partial y\partial t}V_0^2\frac{\partial^3 u}{\partial y^3}\right) + \\ 2(\beta_2+\beta_3)\left(\frac{\partial u}{\partial y}\right)^3 + \gamma_1\left(\frac{\partial^4 u}{\partial y\partial t^3} - 3V_0\frac{\partial^4 u}{\partial y^2\partial t^2} + 3V_0^2\frac{\partial^2 u}{\partial y^3\partial t} - V_0^3\frac{\partial^4 u}{\partial y^4}\right) \\ +2(3\gamma_2+\gamma_3+\gamma_4+\gamma_5+3\gamma_7+\gamma_8)\left(\frac{\partial u}{\partial y}\right)^2\left(\frac{\partial^2 u}{\partial y\partial t} - V_0\frac{\partial^2 u}{\partial y^2}\right) \end{pmatrix}^2\frac{\partial u}{\partial y} \quad (10)$$
$$-\frac{16\sigma^*\theta_\infty^3}{3k^*}\frac{1}{(\rho c_p)_f}\frac{\partial^2\theta}{\partial y^2} + \frac{Q_0}{(\rho c_p)_f}(\theta - \theta_0) + \frac{\mu_f}{(\rho c_p)_f}\left(\frac{\partial u}{\partial y}\right)^2 + \tau\left[D_B\frac{\partial C}{\partial y}\frac{\partial\theta}{\partial y} + \frac{D^T}{\theta_\infty}\left(\frac{\partial\theta}{\partial y}\right)^2\right]$$

ISSN No. 2454-6194 | DOI: 10.51584/IJRIAS |Volume VIII Issue XII December 2023

$$\frac{\partial C}{\partial t}-V_0\frac{\partial C}{\partial y}=D_B\frac{\partial^2 C}{\partial y^2}+\frac{D_m k_T}{\theta_\infty}\frac{\partial^2\theta}{\partial y^2}-Kr\left(C-C_\infty\right),$$

Boundary conditions are

$$At\ y=0,t>0: u(y,t)=U_0V(t)+\lambda_1\left(\mu\frac{\partial u}{\partial y}\right),-k_f\frac{\partial\theta}{\partial y}(y,t)=h_f\left(\theta_f-\theta\right),-D_m\frac{\partial C}{y}(y,t)=h_s\left(C_f-C\right),$$

$$At\ y>0,t=0: u(y,0)=I(y),\frac{\partial u(y,0)}{\partial t}=J(y),\frac{\partial^2 u(y,0)}{\partial t^2}=K(y), \tag{11}$$

$$At\ \ y\to\infty,t>0: u(\infty,t)=0,\theta(y,t)\to\theta_\infty,C(y,t)\to C_\infty,\frac{\partial^n u}{\partial y^n}\to 0,\ \ for\ n=1,2,3$$

Where U_0 is the reference velocity, k_f is the thermal conductivity of the base fluid, α_f is electrical conductivity of base fluid, λ_1 is the slip factor, h_f is the convective heat transfer coefficient, D_m is the molecular diffusivity of the species concentration and h_s is the wall mass transfer coefficient, $V(t),I(y),J(y)$ and $K(y)$ are arbitrary functions. θ_f is the hot fluid temperature, C_f . is the hot fluid concentration, σ^* is the Stefan-Boltzmann constant and k^* is Rosseland mean absorption coefficient, ϕ is the porosity of the porous medium, κ is the permeability of the porous space.

Dimensionless transformation quantities are defined as (Hayat *et al.*, 2009)

$$\bar{u}=\frac{u}{U_0},\bar{y}=\frac{U_0 y}{\nu},\bar{t}=\frac{U_0^2 t}{\nu},\bar{V}=\frac{V_0}{U_0},\bar{\theta}=\frac{\theta-\theta_\infty}{\theta_f-\theta_\infty},\bar{C}=\frac{C-C_\infty}{C_f-C_\infty} \tag{12}$$

Substituting dimensionless quantities in (12) into the dimensional governing equations (9) - (11) gives the non-dimensional system of couple nonlinear partial differential equations (PDEs) as follows

$$\begin{aligned}
&\frac{\partial\bar{u}}{\partial\bar{t}}=\bar{V}_0\frac{\partial\bar{u}}{\partial\bar{y}}+\frac{\partial^2\bar{u}}{\partial\bar{y}^2}+\bar{\alpha}\left(\frac{\partial^3\bar{u}}{\partial\bar{y}^2\partial\bar{t}}-\bar{V}_0\frac{\partial^3\bar{u}}{\partial\bar{y}^3}\right)+\bar{\beta}_1\left(\frac{\partial^4\bar{u}}{\partial\bar{y}^2\partial\bar{t}^2}-2\bar{V}_0\frac{\partial^4\bar{u}}{\partial\bar{y}^3\partial\bar{t}}+\bar{V}_0^2\frac{\partial^4\bar{u}}{\partial\bar{y}^4}\right)+3\bar{\beta}\left(\frac{\partial\bar{u}}{\partial\bar{y}}\right)^2\frac{\partial^2\bar{u}}{\partial\bar{y}^2}+\\
&\bar{\gamma}\left(\frac{\partial^5\bar{u}}{\partial\bar{y}^2\partial\bar{t}^3}-3\bar{V}_0\frac{\partial^5\bar{u}}{\partial\bar{y}\partial\bar{t}^2}-3\bar{V}_0^2\frac{\partial^5\bar{u}}{\partial\bar{y}^4\partial\bar{t}}-\bar{V}_0^3\frac{\partial^5\bar{u}}{\partial\bar{y}^5}\right)+2\bar{\Gamma}\frac{\partial}{\partial\bar{y}}\left[\left(\frac{\partial\bar{u}}{\partial\bar{y}}\right)^2\frac{\partial^2\bar{u}}{\partial\bar{y}\partial\bar{t}}\right]-2\bar{\Gamma}\bar{V}_0\frac{\partial}{\partial\bar{y}}\left[\left(\frac{\partial\bar{u}}{\partial\bar{y}}\right)^2\frac{\partial^2\bar{u}}{\partial\bar{y}^2}\right]\\
&-\phi\begin{pmatrix}\bar{\alpha}\left(\frac{\partial\bar{u}}{\partial\bar{t}}-\bar{V}_0\frac{\partial\bar{u}}{\partial\bar{y}}\right)+\bar{\beta}_1\left(\frac{\partial^2\bar{u}}{\partial\bar{t}^2}-2\bar{V}_0\frac{\partial^2\bar{u}}{\partial\bar{y}\partial\bar{t}}+\bar{V}_0^2\frac{\partial^2\bar{u}}{\partial\bar{y}^2}\right)+\bar{\beta}\bar{u}\left(\frac{\partial\bar{u}}{\partial\bar{y}}\right)^2+\bar{u}\\+\bar{\gamma}\left(\frac{\partial^3\bar{u}}{\partial\bar{t}^3}-3\bar{V}_0\frac{\partial^3\bar{u}}{\partial\bar{y}\partial\bar{t}^2}+3\bar{V}_0^2\frac{\partial^3\bar{u}}{\partial\bar{y}^2\partial\bar{t}}-\bar{V}_0^3\frac{\partial^3\bar{u}}{\partial\bar{y}^3}\right)\\+2\bar{\Gamma}\bar{u}\left(\frac{\partial\bar{u}}{\partial\bar{y}}\right)\left[\frac{\partial^2\bar{u}}{\partial\bar{y}\partial\bar{t}}-\bar{V}_0\left(\frac{\partial^2\bar{u}}{\partial\bar{y}^2}\right)\right]\end{pmatrix}\\
&-\bar{M}^2\bar{u}\sin^2\xi+Gr\bar{\theta}+G_C\bar{C}.
\end{aligned} \tag{13}$$

ISSN No. 2454-6194 | DOI: 10.51584/IJRIAS |Volume VIII Issue XII December 2023

$$\frac{\partial^2\bar{\theta}}{\partial\bar{y}^2}-\left(\frac{\partial\bar{\theta}}{\partial\bar{t}}-\bar{V}_0\frac{\partial\bar{\theta}}{\partial\bar{y}}\right)+\Pr.Ec\left(\begin{array}{l}\bar{\alpha}\left(\frac{\partial^2\bar{u}}{\partial\bar{y}\partial\bar{t}}-\bar{V}_0\frac{\partial^2\bar{u}}{\partial\bar{x}^2}\right)+\bar{\beta}_1\left(\frac{\partial^3\bar{u}}{\partial\bar{y}\partial\bar{t}^2}-2\bar{V}_0\frac{\partial^2\bar{u}}{\partial\bar{y}\partial\bar{t}}+\bar{V}_0^2\frac{\partial^3\bar{u}}{\partial\bar{y}^3}\right)+\\+\bar{\gamma}\left(\frac{\partial^4\bar{u}}{\partial\bar{y}\partial\bar{t}^3}-3\bar{V}_0\frac{\partial^4\bar{u}}{\partial\bar{y}^2\partial\bar{t}^2}+3\bar{V}_0^2\frac{\partial^4\bar{u}}{\partial\bar{y}^3\partial\bar{t}}-\bar{V}_0^3\frac{\partial^4\bar{u}}{\partial\bar{y}^4}\right)+\\2\bar{\Gamma}\left(\frac{\partial\bar{u}}{\partial\bar{y}}\right)^2\left(\frac{\partial^2\bar{u}}{\partial\bar{y}\partial\bar{t}}-\bar{V}_0\frac{\partial^2\bar{u}}{\partial\bar{y}^2}\right)+2\frac{\partial\bar{u}}{\partial\bar{y}}+\bar{\beta}\left(\frac{\partial\bar{u}}{\partial\bar{y}}\right)^3\end{array}\right)\frac{\partial\bar{u}}{\partial\bar{y}}+$$

$$Q\bar{\theta}+Ra\frac{\partial^2\theta}{\partial\bar{y}^2}+Nb\frac{\partial\bar{C}}{\partial\bar{y}}\frac{\partial\bar{\theta}}{\partial y}+Nt\frac{\partial^2\theta}{\partial\bar{y}^2}=0 \tag{14}$$

$$\frac{\partial\bar{C}}{\partial\bar{t}}-\bar{V}_0\frac{\partial\bar{C}}{\partial\bar{y}}=\frac{1}{Sc}\frac{\partial^2\bar{C}}{\partial\bar{y}^2}+Sr\frac{\partial^2\bar{\theta}}{\partial\bar{y}^2}-Kc\bar{C} \tag{15}$$

The dimensionless boundary conditions are

$$At\ \bar{y}=0,\bar{t}>0:\bar{u}(\bar{y},\bar{t})=V(t)+\lambda\left(\frac{\partial\bar{u}}{\partial\bar{y}}\right),-\frac{\partial\bar{\theta}}{\partial\bar{y}}(0,t)=\beta i_1\left(1-\bar{\theta}\right),-\frac{\partial\bar{C}}{\partial y}(0,t)=\beta i_2\left(1-\bar{C}\right),$$

$$At\ \bar{y}>0,\bar{t}=0:\bar{u}(\bar{y},0)=\bar{f}(\bar{y}),\frac{\partial\bar{u}}{\partial\bar{t}}(\bar{y},0)=\bar{g}(\bar{y}),\frac{\partial^2\bar{u}}{\partial\bar{t}^2}(\bar{y},0)=\bar{h}(\bar{y}), \tag{16}$$

$$At\ \bar{y}\to\infty(N),\bar{t}>0:\bar{u}(\bar{y},\bar{t})\to0,\bar{\theta}(\bar{y},t)\to0,\bar{C}(\bar{y},t)\to0,\frac{\partial^n\bar{u}}{\partial\bar{y}^n}\to0,\ for\ n=1,2,3$$

Non-dimenssionalized variables/parameters in equations (13) – (16) are:

$$\bar{\alpha}=\frac{\alpha_1U_0^2}{\rho_f\nu^2},\ \bar{\beta}_1=\frac{\beta_1U_0^4}{\rho_f\nu^3},\ \bar{\beta}=2(\beta_2+\beta_3)\frac{U_0^4}{\rho_f\nu^3},\ \bar{\gamma}=\frac{\gamma_1U_0^6}{\rho_f\nu^4},\ Gr=\frac{\beta_T g\nu(\theta_0-\theta_\infty)}{U_0^3}$$

$$\bar{\Gamma}=(3\gamma_2+\gamma_3+\gamma_4+\gamma_5+3\gamma_7+\gamma_8)\frac{\gamma_1U_0^6}{\rho_f\nu^3},M^2=\frac{\sigma B_0^2\nu}{\rho_f{}^{U_0^2}},\ \bar{\phi}=\frac{\phi\nu^2}{\kappa^{U_0}},\ \bar{f}(y)=\frac{I(y)}{U_0},$$

$$Gc=\frac{\beta_c g\nu(C_0-C_\infty)}{U_0^3},\ \Pr=\frac{\mu f^{C_P}}{k_f},\ \ Ec=\frac{U_0^2}{C_p(\theta_0-\theta_\infty)},\ Q=\frac{\nu^2Q_0}{\alpha_\rho C_P},\ \bar{h}(y)=\frac{K(y)}{U_0} \tag{17}$$

$$Ra=\frac{16\sigma^*\theta_\infty^3}{3k^*\alpha\rho_fC_P},\ Nt=\frac{rD_T(\theta_0-\theta_\infty)}{\alpha\theta_\infty},\ \lambda=\frac{\lambda_1U_0}{\nu},\ Bi_1=\frac{h_f(\theta_0-\theta_\infty)}{kU_0(\theta_{f0}-\theta_\infty)},\ Bi_2=\frac{h_s(C-C_\infty)}{D_BU_0(C_f-C_\infty)}$$

$$Sr=\frac{D_mk_T(\theta_0-\theta_\infty)}{T_\infty\nu(\theta_0-\theta_\infty)},\ Sc=\frac{\nu}{D_B},kc=\frac{\nu Kr}{U_0^2},Nb=\frac{\Gamma D_B(\theta_0-\theta_\infty)}{\alpha_f\theta_\infty},\bar{g}(y)=\frac{J(y)}{U_0}$$

where Ra is the radiation parameter, M is the magnetic parameter, $\bar{\phi}$ is the porosity parameter, Gr is the thermal Grash of number, Sr is the Soret number, Sc is the schmidt number, Kc is the chemical reaction parameter, Nb is the Brownian motion parameter, Nt is the thermophorisis parameter, ξ is the angle of magnetic field inclination, Bi_1 is the thermal biot number, Bi_2 is the concentration Blot number, λ is the slip parameter, Gc is the solutal Grash of number, $\bar{\alpha}$ is the second grade fluid parameter, $\bar{\beta}$ and $\bar{\beta}_1$ are the third grade fluid parameters, γ and Γ are the fourth grade fluid parameters, Q is the heat source parameter, Pr is the Prandtl number, Ec is the Eckert number, N is the infinity(∞) arbitrary value. The function s $\bar{V}(t),\bar{f}(y),\bar{g}(y)$ and $\bar{h}(y)$are dimensionless arbitrary functions.

ISSN No. 2454-6194 | DOI: 10.51584/IJRIAS |Volume VIII Issue XII December 2023

Entropy Generation Analysis

According to Nield and Bejan (2006); Afridi, Qasim, Shafie, and Alshomarani (2017), the modified local volumetric rate of entropy generation describing the problem in the present of magnetic field can be written as

$$S_G = \frac{k_f}{\theta_\infty^2}\left(\frac{\partial\theta}{\partial y}\right)^2 + \frac{\mu_f}{\theta_\infty}\left(\frac{\partial u}{\partial y}\right)^2 + \frac{\sigma_f B_0^2 \sin^2\xi}{\theta_\infty}u^2, \text{ where } \theta_\infty \neq 0 \tag{18}$$

The above volumetric rate of entropy generation equation shows contributions of three sources of entropy generation. The first term represents entropy generation caused by heat transfer along a finite temperature different. However, the second term reveals the local entropy generation due to viscous dissipation, whereas the third term is the local entropy generation due to the effect of the magnetic field. The dimensionless form of entropy generation N_S describes the ratio between the local volumetric entropy generation rate S_G to a characteristic rate of entropy generation S_{G0} .This characteristic entropy generation rate is

$$S_{G0} = \frac{k_f(\Delta\theta)^2}{y^2\theta_\infty^2}, \text{where } \Delta\theta \text{ is difference in fluid temperature.} \tag{19}$$

By taking the ratio of equations (18) and (19). Then, the entropy generation number can be written as $N_s = \frac{S_G}{S_{G0}}$. (20)

Using equations (12), (18) and (19) in (20), then the dimensionless entropy generation number can be written as

$$N_s = \mathrm{Re}^2\left(\frac{\partial\bar{\theta}}{\partial\bar{y}}\right)^2 + \frac{Br\,\mathrm{Re}^2}{\Omega}\frac{\partial\bar{u}}{\partial\bar{y}} + \frac{Br}{\Omega}Ha^2\left(\sin^2\xi\right)\bar{u} \tag{21}$$

where $\mathrm{Re} = \frac{yU_0}{\nu}$, $Br = \frac{\mu_f U_0^2}{k(\theta_0 - \theta_\infty)}$, $\Omega = \frac{(\theta_0 - \theta_\infty)}{\theta_\infty}$, $Ha = B_0 y\sqrt{\frac{\sigma_f}{\mu}}$

Where $\mathrm{Re}, Br, \Omega, Ha, \mu_f$ *and* k_f are the local Reynoids number, Brinkman number, the dimensionless temperature difference, Hartmann number, dynamic viscosity and thermal conductivity respectively.

The physical quantities of engineering interest in this problem are the local skin friction coefficient (surface drag) C_f, the Nusselt number Nu which represents the rate of heat of heat transfer at the surface of the plate and the local Sherwood number Sh describes the rate of mass transfer at the surface of the plate, are defined as

$$C_f = \frac{r_{xy}}{\rho U_0^2}, \quad Nu = \frac{yq_w}{k(\theta_0 - \theta_\infty)}, \quad Sh = \frac{yj_w}{D_B(C_0 - C_\infty)} \tag{22}$$

where, r_{xy} is the wall shear stress, q_w is the heat flux, j_w is the mass flux. These are defined respectively as

$$r_{xy} = \left[\begin{array}{l} \alpha\left(\frac{\partial^2 u}{\partial y\partial t} - V_0\frac{\partial^2 u}{\partial y^2}\right) + \beta_1\left(\frac{\partial^2 u}{\partial y\partial t^2} - 2V_0\frac{\partial^3 u}{\partial y^2\partial t} + V_0^2\frac{\partial^3 u}{\partial y^3}\right) + \\ 2(\beta_2+\beta_3)\left(\frac{\partial u}{\partial y}\right)^3 + \gamma_1\left(\frac{\partial^2 u}{\partial y\partial t^3} - 3V_0\frac{\partial^4 u}{\partial y^2\partial t^2} + 3V_0^2\frac{\partial^4 u}{\partial y^3\partial t} - V_0^3\frac{\partial^4 u}{\partial y^4}\right) + \mu\frac{\partial u}{\partial y} \\ + 2(3\gamma_2 + \gamma_3 + \gamma_4 + \gamma_5 3\gamma_7 + \gamma_8)\left(\frac{\partial u}{\partial y}\right)^2\left(\frac{\partial^2 u}{\partial y\partial t} - V_0\left(\frac{\partial^2 u}{\partial y^2}\right)\right) \end{array}\right]_{y=0} \tag{23}$$

$$q_w = -\left(k_f + \frac{16\sigma^*\theta_\infty^3}{3k^*}\right)\left(\frac{\partial\theta}{\partial y}\right)_{y=0}, \quad j_w = -D_B\left(\frac{\partial C}{\partial y}\right)_{y=0}$$

ISSN No. 2454-6194 | DOI: 10.51584/IJRIAS |Volume VIII Issue XII December 2023

Using equations (12) and (22) in (22), then the dimensionless skin friction coefficient (surface drag), local Nusselt and Sherwood numbers are

$$C_f = \left[\begin{array}{l} \bar{\alpha}\left(\frac{\partial^2 \bar{u}}{\partial \bar{y} \partial \bar{t}} - \bar{V}_0 \frac{\partial^2 \bar{u}}{\partial \bar{y}^2} \right) + \beta_1 \left(\frac{\partial^3 \bar{u}}{\partial \bar{y} \partial \bar{t}^2} - 2\bar{V}_0 \frac{\partial^3 \bar{u}}{\partial \bar{y}^2 \partial \bar{t}} + \bar{V}_0^2 \frac{\partial^3 \bar{u}}{\partial \bar{y}^3} \right) + 2\bar{\Gamma} \left(\frac{\partial \bar{u}}{\partial \bar{y}} \right)^2 \left(\frac{\partial^2 \bar{u}}{\partial \bar{y} \partial \bar{t}} - \bar{V}_0 \left(\frac{\partial^2 \bar{u}}{\partial \bar{y}^2} \right) \right) \\ + \beta \left(\frac{\partial \bar{u}}{\partial \bar{y}} \right)^3 + \bar{\gamma} \left(\frac{\partial^4 \bar{u}}{\partial \bar{y} \partial \bar{t}^3} - 3\bar{V}_0 \frac{\partial^4 \bar{u}}{\partial \bar{y}^2 \partial \bar{t}^2} + 3\bar{V}_0^2 \frac{\partial^4 \bar{u}}{\partial \bar{y}^3 \partial \bar{t}} - \bar{V}_0^3 \frac{\partial^4 \bar{u}}{\partial \bar{y}^4} \right) + \frac{\partial \bar{u}}{\partial \bar{y}} \end{array} \right]_{\bar{y}=0} \tag{24}$$

$$Nu(\mathrm{Re})^{-1/2} = -\vec{\theta}(0,t), \quad SH(\mathrm{Re})^{-1/2} = -\vec{C}(0,t)$$

According to(Aziz et al.,2014), Lie group invariant similarity variable transformation for equations (13) — (15) are respectively defined as

$$u(y,t) = f(\eta), \ \theta(y,t) = q(\eta), \ C(y,t) = \omega(\eta) \ \ with \ \ \eta = y - ct. \tag{25}$$

Where $f(\eta), \ q(\eta) \ and \ \omega(\eta)$ are respectively the arbitrary functions of the flow velocity, temperature and concentration with characteristic variable $\eta = y - ct$.

Substituting (25) into equations (13)-(15). Then, the partial differential equations (13-15) respectively transformed to ordinary differential equations (ODEs) as follows:

$$\begin{array}{l} -(c - V_0)\frac{df}{d\eta} + \frac{d^2 f}{d\eta^2} + \alpha(c - V_0)\frac{d^3 f}{d\eta^3} + \beta_1 (c - V_0)^2 \frac{d^4 f}{d\eta^4} + 3\beta \left(\frac{df}{d\eta} \right)^2 \frac{d^2 f}{d\eta^2} + \gamma (c - V_0)^3 \frac{d^5 f}{d\eta^5} \\ + 2\Gamma (c - V_0) \left(\frac{df}{d\eta} \right)^2 \frac{\mathrm{d}^3 f}{d\eta^3} + 4\Gamma (c - V_0) \frac{df}{d\eta} \left(\frac{d^2 f}{d\eta^2} \right)^2 - fM^2 \sin^2 \xi + Grq + Gc\omega \end{array} \tag{26}$$

$$-\phi \left[\alpha(c - V_0)\frac{df}{d\eta} + \beta_1 (c - V_0)^2 \frac{d^2 f}{d\eta^2} + \beta f \left(\frac{df}{d\eta} \right)^2 + \gamma (c - V_0)^3 \frac{d^3 f}{d\eta^3} + f + 2\Gamma (c - V_0) f \frac{df}{d\eta} \frac{d^2 f}{d\eta^2} \right] = 0$$

$$\begin{array}{l} \frac{d^2 q}{d\eta^2} - \mathrm{Pr}(c - V_0)\frac{dq}{d\eta} + \mathrm{Pr}\, Ec \left[\begin{array}{l} \alpha(c - V_0)\frac{d^2 f}{d\eta^2} + \beta_1 (c - V_0)^2 \frac{d^3 f}{d\eta^3} + \\ \gamma (c - V_0)^3 \frac{d^4 f}{d\eta^4} + 2\Gamma (c - V_0) \left(\frac{df}{d\eta} \right)^2 \frac{d^2 f}{d\eta^2} + \frac{df}{d\eta} + \beta \left(\frac{df}{d\eta} \right)^3 \end{array} \right] \left(\frac{df}{d\eta} \right) \\ + Qq + Ra \frac{d^2 q}{d\eta^2} + Nb \frac{dw}{d\eta} \frac{dq}{\partial \eta} + Nt \frac{d^2 q}{d\eta^2} = 0 \end{array} \tag{27}$$

$$-c\frac{dw}{d\eta} - \bar{V}_0 \frac{dw}{d\eta} = \frac{1}{Sc} \frac{d^2 \omega}{d\eta^2} + Sr \frac{d^2 q}{d\eta^2} - Kc\omega \tag{28}$$

The boundary conditions become:

$$\begin{array}{l} At \ \ \eta = 0, \ \ f(\eta) = -1 + \lambda \left(\frac{df}{d\eta} \right), \frac{df}{d\eta} = -Bi_1 (1 - q), \frac{dw}{d\eta} = -Bi_2 (1 - w) \\ As \ \eta \to \infty (N), \ \ f(\eta) \to 0, \ q(\eta) \to 0, \ w(\eta) \to 0, \ \frac{d^n f}{d\eta^n} \to 0, \ \ for \ n = 1,2,3 \end{array} \tag{29}$$

ISSN No. 2454-6194 | DOI: 10.51584/IJRIAS |Volume VIII Issue XII December 2023

III. Method of Solution by Homotopy Perturbation method

It is very difficult to develop a closed-form solution for the above non-linear equation Equations (26)-(28) subject to boundary condition (29). Therefore, recourse has to be made to either an approximation analytical method, semi-numerical method or numerical method of solution. In this work, homotopy perturbation method is used to solve the equation.HPM is used due to its comparative advantages and the provision of acceptable analytical results with convenient convergence and stability coupled with total analytical procedures. According to homotopy perturbation method (HPM) procedure highlighted inHe, 2003 and 2006; Xu, 2007; Hoshyar et al., 2015), one can construct a homotopy for equations (26) -(28) as follows

$$H_1(p,\eta)=(1-p)\left[\gamma(c-V_0)^3\frac{d^5f}{d\eta^5}\right]+$$

$$p\left[\begin{array}{l}-(c-V_0)\dfrac{df}{d\eta}+\dfrac{d^2f}{d\eta^2}+\alpha(c-V_0)\dfrac{d^3f}{d\eta^3}+\beta_1(c-V_0)^2\dfrac{d^4f}{d\eta^4}+3\beta\left(\dfrac{df}{d\eta}\right)^2\dfrac{d^2f}{d\eta^2}+\gamma(c-V_0)^3\dfrac{d^3f}{d\eta^3}\\ +2\Gamma(c-V_0)\left(\dfrac{df}{d\eta}\right)^2\dfrac{d^3f}{d\eta^3}+4\Gamma(c-V_0)\dfrac{df}{d\eta}\left(\dfrac{d^2f}{d\eta^2}\right)^2-M^2f\sin^2\xi+Grq+Gcq\\ -\phi\left[\alpha(c-V_0)\dfrac{df}{d\eta}+\beta_1(c-V_0)^2\dfrac{d^2f}{d\eta^2}+\beta f\left(\dfrac{df}{d\eta}\right)^2+\gamma(c-V_0)^3\dfrac{d^3f}{d\eta^3}+f+2\Gamma(c-V_0)f\dfrac{df}{d\eta}\dfrac{d^2f}{d\eta^2}\right]\end{array}\right]=0 \quad (30)$$

$$H_2(p,\eta)=(1-p)\left[(1+Ra+Nt)\frac{d^2q}{d\eta^2}\right]+$$

$$p\left[\begin{array}{l}\dfrac{d^2q}{d\eta^2}-\Pr(c-V_0)\dfrac{dq}{d\eta}+\Pr Ec\left[\begin{array}{l}\alpha(c-V_0)\dfrac{d^2f}{d\eta^2}+\beta_1(c-V_0)^2\dfrac{d^3f}{d\eta^3}+\\ \gamma(c-V_0)^3\dfrac{d^4f}{d\eta^4}+2\Gamma(c-V_0)\left(\dfrac{df}{d\eta}\right)^2\dfrac{d^2f}{d\eta^2}+\dfrac{df}{d\eta}+\beta\left(\dfrac{df}{d\eta}\right)^3\end{array}\right]\left(\dfrac{df}{d\eta}\right)\\ +Qq+Ra\dfrac{d^2q}{d\eta^2}+Nb\dfrac{d\omega}{d\eta}\dfrac{dq}{\partial\eta}+Nt\dfrac{d^2q}{d\eta^2}\end{array}\right]=0 \quad (31)$$

$$H_3(p,\eta)=(1-p)\left[\frac{1}{Sc}\frac{d^2\omega}{d\eta^2}\right]+p\left[c\frac{d\omega}{d\eta}+\bar{V}_0\frac{d\omega}{d\eta}+\frac{1}{Sc}\frac{d^2\omega}{d\eta^2}+Sr\frac{d^2f}{d\eta^2}+Kc\omega\right]=0 \quad (32)$$

Taking respective power series of flow velocity, temperature and concentration fields in equations (26-28) as

$$f(\eta)=f_0(\eta)+pf_1(\eta)+p^2f_2(\eta)+p^3f_3(\eta) \quad (33)$$

$$q(\eta)=q_0(\eta)+pq_1(\eta)+p^2q_2(\eta)+p^3q_3(\eta) \quad (34)$$

$$\omega(\eta)=\omega_0(\eta)+p\omega_1(\eta)+p^2\omega_2(\eta)+p^3\omega_3(\eta) \quad (35)$$

Substituting equation (33), (34) and (35) into equations (30), (31) and (32), then separating and collecting like terms in order of power of p^0, p^1, p^2, p^3 and apply the boundary conditions (29) in accordance with HPM's rule. Thereafter, maple mathematical software is used to generate the expressions for

$f_0(\eta), q_0(\eta), \omega_0(\eta), f_1(\eta), q_1(\eta), \omega_1(\eta), f_2(\eta), q_2(\eta), \omega_2(\eta), f_3(\eta), q_3(\eta)$ *and* $\omega_3(\eta)$ in equations (33-35) as

ISSN No. 2454-6194 | DOI: 10.51584/IJRIAS |Volume VIII Issue XII December 2023

$$f_0 = \frac{\eta^4}{(N+4\lambda)N^3} - \frac{4\eta^3}{(N+4\lambda)N^2} + \frac{6\eta^2}{(N+4\lambda)N} - \frac{4\eta}{(N+4\lambda)} - \frac{4\eta}{N+4\lambda} + 1 \tag{36}$$

$$q_0 = -\frac{Bi_1}{(NBi_1 - 1)}\eta + \frac{NBi_1}{(NBi_1 - 1)} \tag{37}$$

$$\omega_0 = -\frac{Bi_2}{(NBi_2 - 1)}\eta + \frac{NBi_2}{(NBi_2 - 1)} \tag{39}$$

Expression for $f_1(\eta), q_1(\eta), \omega_1(\eta), f_2(\eta), q_2(\eta), \omega_2(\eta), f_3(\eta), q_3(\eta)$ *and* $\omega_3(\eta)$ obtained from maple mathematical software are too long to displace here, but they are included in the simulated results shown graphically and tabularly under results and discussion.

By substituting equations (36)-(39) and $f_1(\eta), q_1(\eta), \omega_1(\eta), f_2(\eta), q_2(\eta), \omega_2(\eta), f_3(\eta), q_3(\eta)$ into equations (33)-(35) and set p=l. Then, with aid of Maple mathematical software, one respectively obtained the solutiors for fluid flow velocity $f(\eta)$ temperature distribution $\omega(\eta)$ and concentration $C(\eta)$ fields as follows

$$f(\eta) = \left[\frac{-1\gamma\beta_1\phi(c-V_0)M^2\sin^2\xi}{21(N+4\lambda)}\right]^3\left(\frac{\eta^5}{21} - \frac{\eta^6}{20} - \frac{\eta^7}{31} - \frac{\eta^8}{50}\right)^4 + \left[\frac{cRa\Gamma\alpha Gc}{(NBi_1 - 1)} + \frac{\phi MNBiGr}{(NBi_1 - 50)}\right]^3\left(\frac{\eta^6}{31} - \frac{\eta^7}{35} - \frac{\eta^8}{60}\right)^2$$

$$\frac{((c-V_0)Ra\gamma\lambda)^2}{ScNnBi_2\gamma Q}\Pr\left(\frac{GrGc}{42}(20\Pr - 2Q)\eta^4 + \frac{1}{70}(Ec\Pr + 143)\eta + \frac{Nb}{Nt}\right)^2 + \frac{(Sr-Kc)}{Sc-Sr}\left(\frac{1}{2}\eta^2 - \frac{\eta^6}{2}\right)^5$$

$$-\frac{Bi_2cSr\eta}{(NBi_2 - 1)} + \frac{ScNnBi_2\gamma}{(NBi_2 - 1)}\left(\frac{\eta^6}{2} - \frac{\eta^7}{2}\right)^2 + \frac{5cBi_1Bi_2\lambda}{\Gamma(N+4\lambda)N^3} - \frac{NtNGrGc}{(N+4\lambda)N^2} + \frac{23Ec}{67899}\eta^8 + (\cos^2\xi Sin^2\xi)^2$$

$$+\left(\frac{1}{42}(-20\Pr - 2M^2Q)\eta^4 + \frac{1}{12}(6\lambda\Pr + 6543)\eta - NbNt + \frac{Nb}{Nt}\right)^2 + \frac{M^2Sin^2\xi}{NBi_1 - 1}\left(\frac{\eta^{10}}{2} - \frac{\eta^9}{2} - \frac{\eta^8}{2}\right)^2 + \frac{\eta^8}{232}$$

$$+\frac{M^2Sin^2\xi}{NBi_1 - 1}\left(\frac{\eta^{10}}{2} - \frac{\eta^9}{2} - \frac{\eta^8}{2}\right)^2 + \frac{M^2Sin^2\xi}{NBi_1 - 1}\left(\frac{\eta^{10}}{2} - \frac{\eta^9}{2} - \frac{\eta^8}{2}\right)^2 - \frac{M^2Sin^2\xi}{NBi_1 - 1}\left(\frac{\eta^{10}}{2} - \frac{\eta^9}{2} - \frac{\eta^8}{2}\right)^2 + \frac{M^2Sin^2\xi}{NBi_1 - 1}$$

$$-\frac{Q(Ec - \Pr)}{50 - 2\Pr}\left(\frac{\eta^5}{10} - \frac{\eta^6}{22} - \frac{\eta^7}{23} - \frac{\eta^8}{24}\right)^2 + M^2Kc\left(\frac{Nt-P}{Nb}\right)^2\frac{NBi_1Bi_1\eta Sin^2\xi\cos^2\xi}{NBi_1 - 1}\left(\frac{\eta^2}{10} - \frac{\eta^3}{22} - \frac{\eta^4}{23} - \frac{\eta^5}{24}\right)^2$$

$$-\frac{Q(Ec - \Pr)}{50 - 2\Pr}\left(\frac{\eta^5}{10} - \frac{\eta^6}{22} - \frac{\eta^7}{23} - \frac{\eta^8}{24}\right)^2 + \frac{M^2Kc}{\lambda Kc}\left(\frac{Nt-c}{M^2Kc}\right)^2\frac{NBi_1Bi_1\eta Sin^2\xi\cos^2\xi}{NBi_1 - 1}\left(\frac{\eta^2}{10} - \frac{\eta^3}{22} - \frac{\eta^4}{23} - \frac{\eta^5}{24}\right)^3$$

+.....

$$q(\eta) = -\frac{Q(Ec - \Pr)}{50 - 2\Pr}\left(\frac{\eta^5}{200} - \frac{\eta^6}{22} - \frac{\eta^7}{215} - \frac{\eta^8}{144}\right)^2 + \frac{M^2\lambda Kc}{Nt - Nb}\left(\frac{Nt - Ec}{Nb - N}\right)^2\frac{NBi_1Ra\cos 5\xi}{(NBi_1 - 1)}\left(\frac{\eta^4}{10} - \frac{\eta^5}{22} - \frac{\eta^6}{23} - \frac{\eta^3}{24}\right)^2$$

$$-\frac{Q(Ec - \Pr)}{50 - 2\Pr}\left(\frac{\eta^5}{10} - \frac{\eta^6}{22} - \frac{\eta^7}{23} - \frac{\eta^8}{24}\right)^2 + \frac{\lambda GrGc}{M\sin^2\xi}\left(\frac{Nt - Q}{Nb - N}\right)^2\frac{NBi_1Bi_1\lambda - \cos^2\xi}{(NBi_1 - 1)}\left(\frac{\eta^4}{110} - \frac{\eta^5}{120} - \frac{\eta^6}{23} - \frac{\eta^3}{24}\right)^2$$

$$-\frac{\frac{Nt\lambda}{3Nb}Q(c - V_0) + \frac{Sc}{Nb}}{50 - 2\Pr}\left(\frac{\eta^2}{122} - \frac{\eta^3}{150} - \frac{\eta^5}{210}\right)^2 + \frac{V_0Nb}{RaSc}\left(\frac{\gamma N - Ec}{Kc - N}\right)^2 - \left(\frac{\Gamma\alpha Sin^2\xi}{(NBi_2 - Kc)} - \frac{\lambda Bi_1M^2}{Kc - Sc} + \frac{Bi_2SrM^2}{Kc - Sc}\right)^2$$

$$-\frac{Q(c - V_0)}{34 - 5\Pr}\left(\frac{\eta^5}{23} - \frac{\eta^6}{100} - \frac{\eta^7}{34} - \frac{\eta^8}{14}\right)^2 + \frac{\beta Gr}{Ra - Gc}\left(\frac{Nt - \Pr}{Nb - N}\right)^2\frac{\Gamma\alpha Sin^2\xi}{(NBi_2 - 1)}\left(\frac{\eta^4}{12} - \frac{\eta^5}{105} - \frac{\eta^6}{24} - \frac{\eta^7}{56}\right)^2\frac{\eta^2}{20}$$

$$-\frac{Q(Ec - \Pr)}{91 - 2Ec}\left(\frac{\eta^5}{10} - \frac{\eta^4}{212} - \frac{\eta^6}{23}\right)^2 + \left(NtKc\left(\frac{M-c}{Nb-N}\right)^3\frac{N\lambda Bi_1 - \cos^2\xi - Sin^2\xi}{(NBi_2 - 1)}\left(\frac{\eta^5}{22} - \frac{\eta^6}{23} - \frac{\eta^7}{24}\right)^2\right)^2 + ...$$

ISSN No. 2454-6194 | DOI: 10.51584/IJRIAS |Volume VIII Issue XII December 2023

$$\omega(\eta)=\frac{Qc\lambda(c-V_0)}{50-2Ec\,\Pr}\left(\frac{\eta^5}{23}-\frac{\eta^6}{100}-\frac{\eta^7}{34}-\frac{\eta^8}{14}\right)^2+M^2\beta\left(\frac{Nt-N}{Nb-8}\right)^3\frac{\Gamma\gamma Bi_1 Sin^2\xi\cos^2\xi}{(NBi_1-M)}\left(\frac{\eta}{12}-\frac{\eta^2}{105}-\frac{\eta^3}{24}-\frac{\eta^6}{56}\right)^2$$
$$-\frac{Qc(EcRa)}{100-2\,\Pr}\left(\frac{\eta^2}{10}-\frac{\eta^3}{22}-\frac{\eta^4}{23}-\frac{\eta^5}{24}\right)^2+\left(\frac{cM^2\lambda Kc}{Gr}\left(\frac{Nt-Gc}{Nb-6}\right)^3\left(\frac{NBi_1-\cos^2\xi Sin^2\xi}{(NBi_1-M)}\right)\left(\frac{\eta^2}{22}-\frac{\eta^3}{30}-\frac{\eta^4}{72}\right)^2\right)^2$$
$$-\frac{SrNt(c-V_0)Q}{SrKc-Sc}\left(\frac{\eta}{105}-\frac{\eta^2}{107}-\frac{\eta^4}{467}\right)^2+M^2Kc\frac{Nt}{Nb}\left(\frac{\gamma Nt-Q}{Nb+6}\right)^2-\frac{\Gamma\alpha Sin^2\xi}{(NBi_2-Sr)}-\frac{\lambda Bi_1M^2}{Kc-Sc}+\frac{Bi_2SrM^2}{Kc-Sc}$$
$$-\frac{Q\lambda(c-V_0)}{70-2\,\Pr}\left(\frac{\eta^2}{13}-\frac{\eta^3}{120}-\frac{\eta^4}{56}-\frac{\eta^5}{56}\right)^2+M^2Sr\left(\frac{Nt-\Gamma}{Nb+4}\right)^2\frac{\Gamma\gamma NtSin^3\xi-\cos^3\xi}{(NBi_1-Sc)}\left(\frac{\eta^2}{12}-\frac{\eta^3}{105}-\frac{\eta^4}{24}-\frac{\eta^5}{56}\right)^2$$
$$-\frac{\Gamma(Ec-\Pr)}{N-Ec\,\Pr}\left(\frac{\eta^5}{10}-\frac{\eta^6}{212}-\frac{\eta^7}{213}\right)^2+\left(M^2Sc\left(\frac{Nt-M}{Nb-4}\right)^2\frac{N\lambda Bi_2-MGr\cos^{2\xi}}{(NBi_2-1)}\left(\frac{\eta}{127}-\frac{\eta^2}{143}-\frac{\eta^3}{64}\right)^5\right)^2+.....$$

Part of the solutions in $f(\eta)$, $q(\eta)$ and $\omega(\eta)$ above have been truncated because they are too long to display here. However, the complete solutions are used in the simulated results shown graphically and tabularly under results and discussion.

IV. Results and Discussion

The default parameter values used in this research to plot graph and generate tables are $\alpha=1,\ \beta_1=0.5,\ \Gamma=1,\gamma=1,\ V_0=1,\Pr=0.75,\ Ec=1.0,\ Gr=2,\ Gc=1,\ \phi=0.2,\ M=1,\ N=20,\ Sc=2.1,\ Sr=0.2,$ $Kc=1,\ Ra=1,\ Bi_1=0.1,\ Q=2,\ c=1.5,\ Bi_2=0.1,\ Nt=1.0,\ Nb=1.0,\ \lambda=1.5$

In order to established the accuracy of HPM solutions, all the results obtained via HPM are verified by comparing with numerical method results using shooting method alongside the six-order Runge-Kutta method (RKM). The code is impelemented with the aid of maple mathematical software. An excellent agreement is found between the two sets of results. Thus, this can be seen as absolute difference between the two set of results, at every points tends to zero in Tables 1-6 under results and discussion section. Thereore, the use of semi-analytical approach via homptopy perturbation method (HPM) in this research work is justified.

4.1. Effects of Embedded flow parameters on Skin friction coefficient, wall heat and mass transfer rates

Table 1:Computational effectsof unsteady parameter c, magnetic parameter M, thermal Grashof number Gr on skin friction coefficient, wall heat transfer and wall mass transfer rates.

		$-f'(0)$			$-q'(0)$			$-\omega'(0)$		
PP	values	HPM	RKM	|HPM-RKM|	HPM	RKM	|HPM-RKM|	HPM	RKM	|HPM-RKM|
c	1.0	0.796650	0.796629	0.0000215	0.645125	0.645100	0.0000252	0.089870	0.089849	0.0000213
	2.0	0.989910	0.989894	0.0000158	0.832310	0.832299	0.0000110	0.097890	0.097866	0.0000244
	3.0	1.278190	1.278179	0.0000110	0.925410	0.925389	0.0000213	0.148090	0.148024	0.0000658
M	0.5	0.698675	0.698635	0.0000405	0.993550	0.993527	0.0000235	0.512230	0.512215	0.0000150
	1.5	0.935894	0.935860	0.0000340	0.743560	0.743519	0.0000408	0.343210	0.343195	0.0000147
	2.5	1.017880	1.017868	0.0000124	0.567890	0.567878	0.0000117	0.106541	0.106510	0.0000313
Gr	1.0	0.698176	0.698164	0.0000121	0.912345	0.912313	0.0000325	1.289150	1.289082	0.0000680
	3.0	0.809918	0.809895	0.0000230	0.811380	0.811364	0.0000157	1.075460	1.075444	0.0000160
	5.0	1.141556	1.141513	0.0000431	0.554660	0.554649	0.0000107	0.926570	0.926521	0.0000490

ISSN No. 2454-6194 | DOI: 10.51584/IJRIAS |Volume VIII Issue XII December 2023

Table 1 shows the effects of unsteady parameter c, thermal Grash of number Gr, magnetic parameters M on skin friction coefficient $-f'(0)$, wall heat transfer rate $-q'(0)$ and wall mass transfer rate $-\omega'(0)$. Increasing the value of unsteady parameter c increases the skin friction coefficient, wall heat transfer and wall mass transfer rate. On the other hand, both Grashof number Gr and magnetic parameter M retard heat transfer and mass transfer rates whereas these parameters enhance the skin friction coefficient.

Table2: Computaional effects of Suction/Injection (V_0>0/ V_0< 0) parameter, thermal radiation parameter Ra, and Brownianmotion parameter Nb on skin friction coefficient, wall heat transfer and wall mass transfer rates

		$-f'(0)$			$-q'(0)$			$-\omega'(0)$		
PP	Values	HPM	RKM	$\lvert HPM-RKM\rvert$	HPM	RKM	$\lvert HPM-RKM\rvert$	HPM	RKM	$\lvert HPM-RKM\rvert$
V_0	-0.3	0.316950	0.316939	0.0000113	0.217650	0.217618	0.0000319	0.109543	0.109531	0.0000122
	-0.1	0.435580	0.435567	0.0000134	0.345610	0.345588	0.0000217	0.180097	0.180084	0.0000126
	0.0	0.577809	0.577798	0.0000115	0.510345	0.510274	0.0000712	0.265099	0.265076	0.0000233
	0.3	0.689819	0.689788	0.0000312	0.754961	0.754921	0.0000400	0.324546	0.324545	0.0000011
Ra	0.2	0.797650	0.797639	0.0000111	0.545450	0.545416	0.0000340	1.164700	1.164619	0.0000811
	0.3	0.678091	0.678050	0.0000411	0.474510	0.474459	0.0000511	1.190989	1.190966	0.0000233
	0.5	0.559819	0.559807	0.0000121	0.274961	0.274941	0.0000200	1.248100	1.248058	0.0000421
Nb	0.0	0.678620	0.678600	0.0000202	0.661230	0.661133	0.0000970	0.409130	0.409038	0.0000921
	0.5	0.407818	0.407799	0.0000195	0.506788	0.506698	0.0000897	0.561206	0.561113	0.0000931
	1.0	0.281979	0.281958	0.0000202	0.447545	0.447489	0.0000560	0.789915	0.789863	0.0000525

Effects of suction velocity $V>0$, thermal radiation parameter Ra and Brownian motion parameter Nt on skin friction, heat transfer and mass transfer rates at the wall are shown in **Table 2**. It is observed from the table that the enhanced values of suction parameter leads to increase in skin friction, heat transfer and mass transfer rates at the wall. On the other hand, both thermal radiation Ra and Brownian motion (Nt) parameters enhance mass transfer rate while these parameters reduce both skin friction coefficient and heat transfer rates.

Table 3:Computaional effects of thermophoresis parameter Nt, Prandtl number Pr and heat source parameter Q on skin friction coefficient, wall heat transfer and wall mass transfer rates

		$-f'(0)$			$-q'(0)$			$-\omega'(0)$		
pp	Values	HPM	RKM	$\lvert HPM-RKM\rvert$	HPM	RKM	$\lvert HPM-RKM\rvert$	HPM	RKM	$\lvert HPM-RKM\rvert$
Nt	1.0	0.789215	0.789185	0.0000301	0.986500	0.986482	0.0000184	0.518900	0.518859	0.0000410
	2.0	0.678480	0.678440	0.0000402	0.678012	0.677982	0.0000306	0.432170	0.432129	0.0000412
	3.0	0.520120	0.520090	0.0000304	0.521905	0.521883	0.0000222	0.324569	0.324552	0.0000171
Pr	0.7	0.439743	0.439732	0.0000112	0.789560	0.789550	0.0000100	0.444440	0.444405	0.0000347
	1.5	0.568320	0.568277	0.0000431	0.985432	0.985391	0.0000412	0.208525	0.208513	0.0000116
	2.5	0.674321	0.674270	0.0000514	1.087644	1.087632	0.0000121	0.109532	0.109501	0.0000311
Q	0.2	0.678930	0.678915	0.0000149	1.209854	0.809849	0.0000123	0.926570	0.926473	0.0000973
	0.5	0.345612	0.345522	0.0000899	0.987540	0.987522	0.0000176	1.075460	1.075443	0.0000171
	0.8	0.103220	0.103184	0.0000354	0.809860	0.809849	0.0000112	1.289150	1.289082	0.0000678

Table 3 shows the influence of thermpphoresis parameter Nt, Prandtl number Pr and heat source parameter Q on skin friction, Nusselt number and Sherwood number. Thermophoresis parameter Nt reduces skin friction, heat transfer and mass transfer rates. However, increasing the values of Prandtl number leads to increase in both skin friction coefficient and heat transfer rate while it decreases mass transfer rate. This is due to the fact that the higher the Prandtl number, the thinner the thermal boundary layer and the thicker the nanoparticle volume fraction boundary layer. As a result of this, the rate of heat diffusion increases while the rate of mass diffusion decreases with increasing values of Prandtl Pr. On the other hand, increasing the values of heat source

ISSN No. 2454-6194 | DOI: 10.51584/IJRIAS |Volume VIII Issue XII December 2023

parameter Q results in reducing both the skin friction coefficient and heat transfer rate whereas it makes mass transfer rate increase more.

Table 4: Computation effects of Eckert number Ec, chemical reaction parameter, Kc and Schmidt number Sc on Skin friction coefficient, wall heat and wall mass transfer rates

		$-f'(0)$			$-q'(0)$			$-\omega'(0)$		
PP	Values	HPM	RKM	|HPM-RKM|	HPM	RKM	|HPM-RKM|	HPM	RKM	|HPM-RKM|
Ec	0.0	0.843200	0.843184	0.0000161	0.996420	0.996399	0.0000214	0.234876	0.234866	0.0000104
	0.5	0.809860	0.809844	0.0000156	0.801245	0.801235	0.0000103	0.376210	0.376154	0.0000561
	1.0	0.782134	0.782123	0.0000111	0.701240	0.701229	0.0000104	0.432120	0.4321100	0.0000100
Kc	0.5	0.875430	0.875420	0.0000103	0.291230	0.291189	0.0000412	0.643200	0.643150	0.0000503
	1.0	0.849041	0.848990	0.0000511	0.250148	0.250107	0.0000413	0.752162	0.752141	0.0000209
	1.0	0.801233	0.801223	0.0000101	0.217630	0.217614	0.0000164	0.900100	0.900079	0.0000208
Sc	0.0	0.348901	0.348845	0.0000561	0.964091	0.963996	0.0000949	0.686321	0.686260	0.0000614
	0.5	0.239008	0.238927	0.0000810	0.890179	0.890089	0.0000895	0.878906	0.878816	0.0000900
	1.0	0.197633	0.197585	0.0000482	0.764325	0.764244	0.0000816	0.901230	0.901216	0.0000145

Table 4shows the effects of Eckert number Ec, chemical reaction parameter Kc, and Schmidt number Sc, on skin friction, wall heat transfer and wall mass transfer rates. As it is clearly shown, Ec and Sc reduce both skin friction and Nusselt number while both parameters increase mass transfer rates. However, chemical reaction parameter retards both the skin friction coefficient and heat transfer rate whereas it enhances mass transfer rate.

Here, the effects of each of the embedded flow parameters on velocity field are presented in figures 2-15.

Figure 2 shows the influence of magnetic field parameter M on the velocity profiles. It is observed that the velocity profile decreases with an increase in the value of the magnetic field parameter M. This is because the imposition of the magnetic in an electrically conducting fluid induces a drag-like force known as Lorentz force on the flow field which acts against the fluid motion and slows it down. Thus, Lorentz force increases as M increases which then dampens the velocity profile. The presence of magnetic field reduces the velocity throughout the boundary layer which is in conformity with the fact that the Lorentz force (magnetic force) acts as a retarding force and, consequently, it reduces the momentum boundary layer thickness significantly

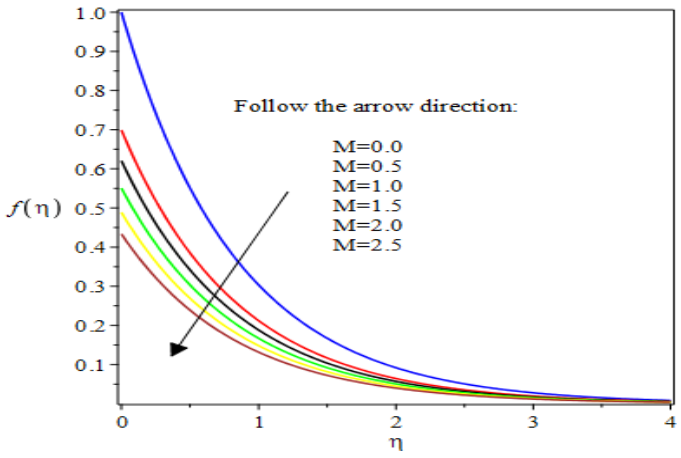

Fig.2.Effects of M on velocity profile

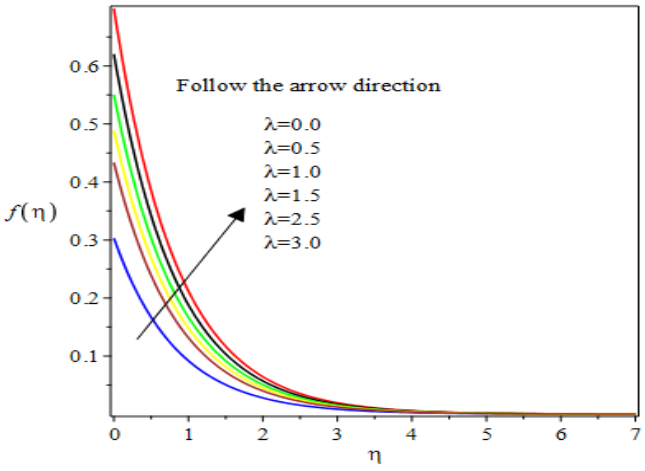

Fig.3.Effectof λ on velocity profile

ISSN No. 2454-6194 | DOI: 10.51584/IJRIAS |Volume VIII Issue XII December 2023

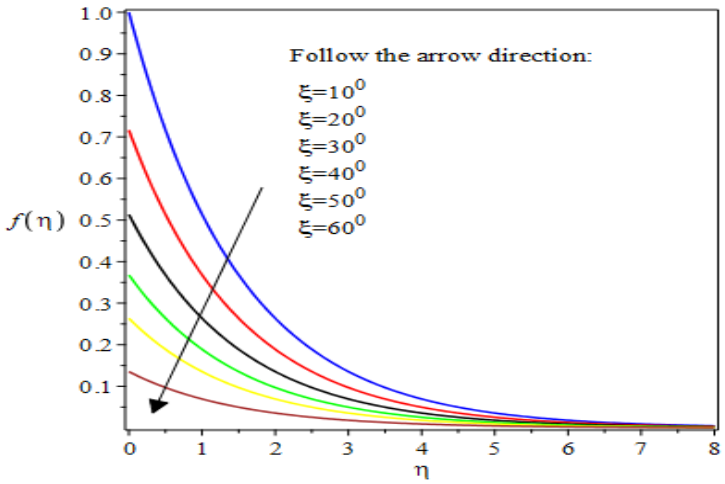

Fig. 4. Effects of ξ on velocity profile

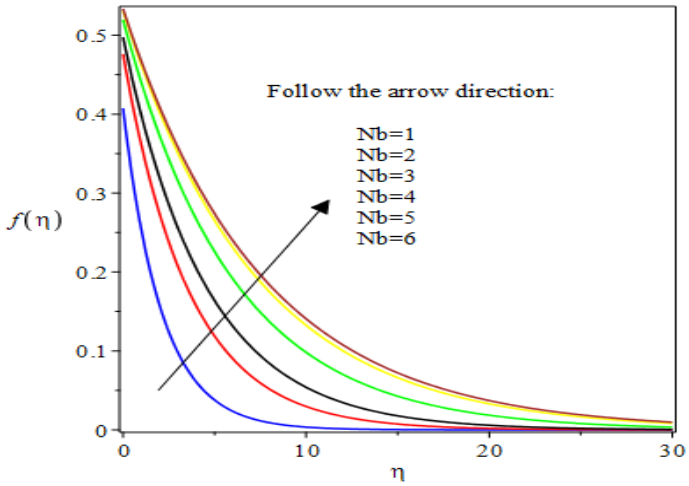

Fig. 5. Effects of Nb on velocity profile

The effects of slip on the velocity profiles when other flow parameters are kept constant can be seen in fig.3As expected, an increase in slip parameter resulted in an increase in the flow velocity near the surface of the plate. The velocityapproaches zero at a distance far off from the plate with an increase in the slip in accordance with the boundary condition. Figure 4 shows the velocity distributions for different angles (ξ) of inclination of the magnetic. A rise in the degree of angle of magnetic inclination ξ, resulted in an increase in the effect of the buoyancy force and thereby reduces the force driven the fluid flow. Consequently, flow velocity decreases.The effects of the Brownian motion parameter (Nb) on velocity profile is illustrated in Figure 5. Brownian motion is therandom motion of suspended nanoparticles in the base fluid and is more influenced by fast moving atoms or molecules in the base fluid. It is worth mentioning that Brownian motion is related to the size of the nanopartcles and are often in the form of agglomeration. The hydrodynamic boundary layer thickness improves as the values of the Brownian motion parameter Nb increases. Brownian motion parameter

Nb enhances the velocity profiles ignificantly. That is, increase in Brownian motion leads to increase in flow velocity.

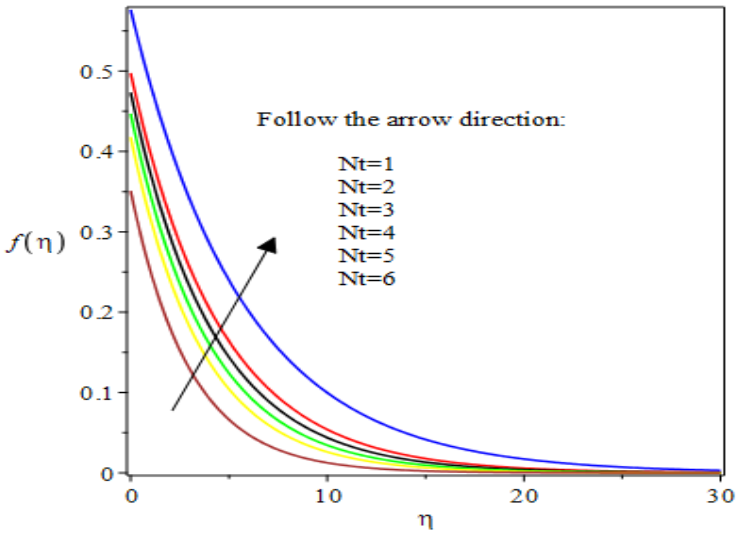

Fig.6.Effects of Nt on velocity profile

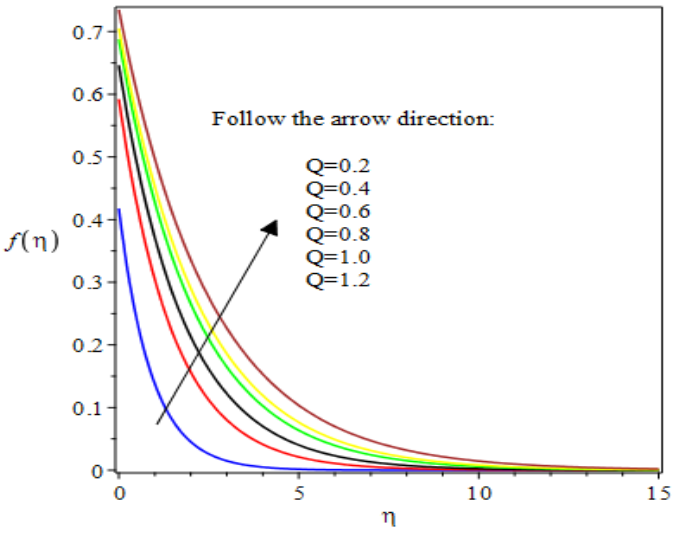

Fig.7.Effects of Q on velocity profile

ISSN No. 2454-6194 | DOI: 10.51584/IJRIAS |Volume VIII Issue XII December 2023

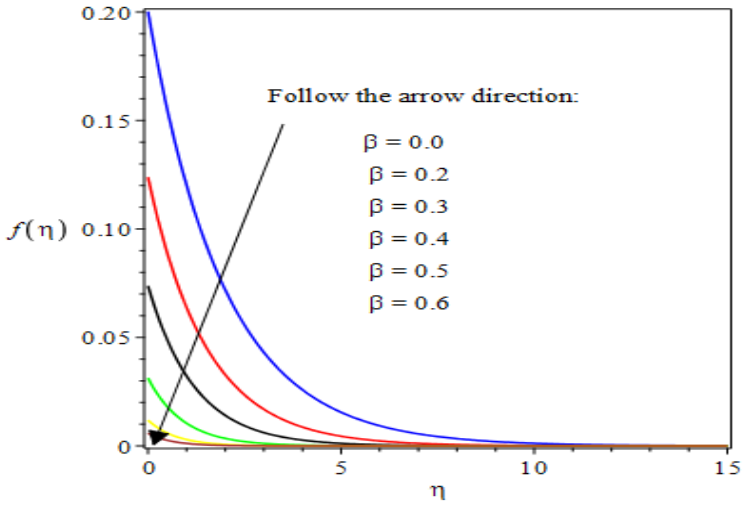

Fig. 8. Effects of β on velocity profile

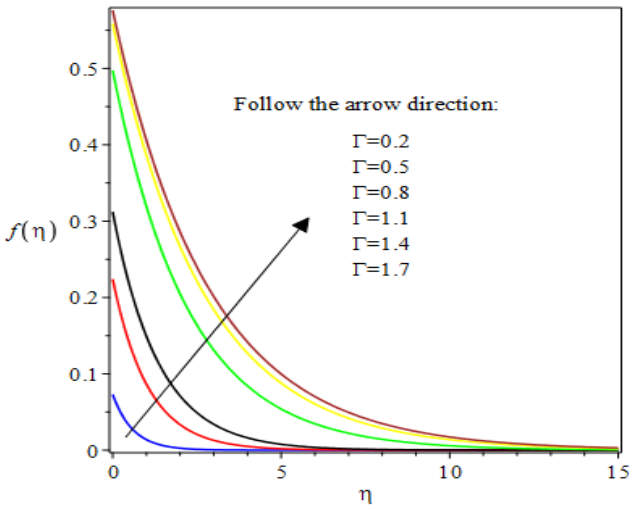

Fig.9. Effects of Γ on velocity profile

Figure 6 shows the effects of thermophoresis parameter Nt on velocity profile. The increments inNt parameter assist the velocity profile to grow. This is because of the fact that particles near the hot surface create thermophorectic force; this force enhances the temperature of the fluid in the boundary layer region. Figure 7 depicts the effect of heat source parameter Q on velocity profile. This parameter enhances velocity of the flow significantly.This is due to the fact that increase in heat source allows more energy to flow into the fluid thereby result in fluid acceleration. In order to describe the influence of the third grade parameter β and fourth grade parameter Γ on the flow model, the velocity profiles have been plotted in Figs. 8 and 9. As anticipated, these figures reveal that both β and Γ have opposite roles on the structure of the velocity, i.e,with an increase in parameter β, the velocity field is decreasing, which shows the shear thickening behaviour of the fluid. However, the velocity profile increases for increasing values of Γ showing the shear thinning property of the fluid.

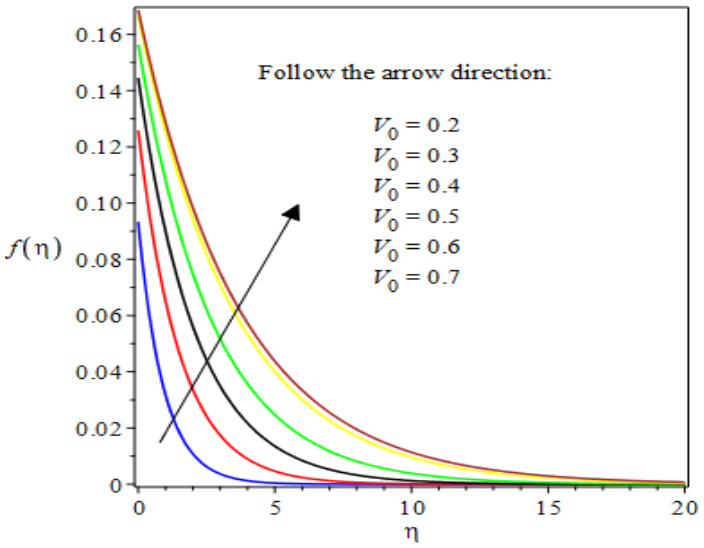

Fig.10. Effects of V_0 on velocity profile

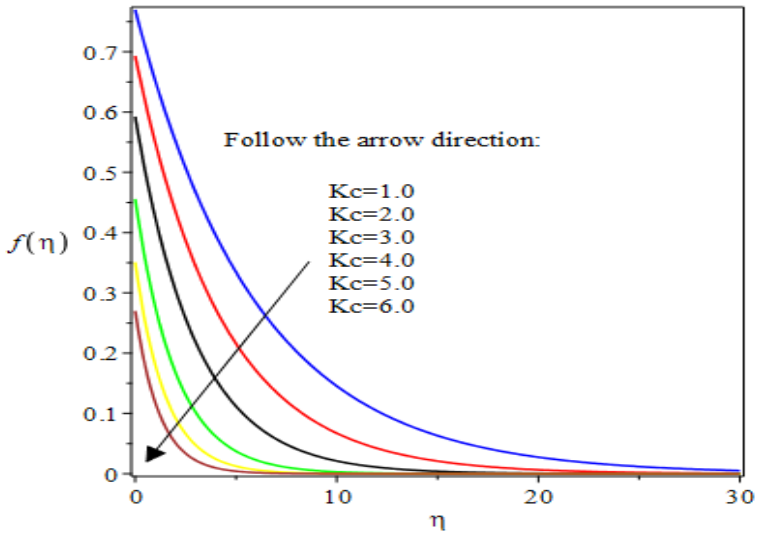

Fig.11. Effects of Kc on velocity profile

ISSN No. 2454-6194 | DOI: 10.51584/IJRIAS |Volume VIII Issue XII December 2023

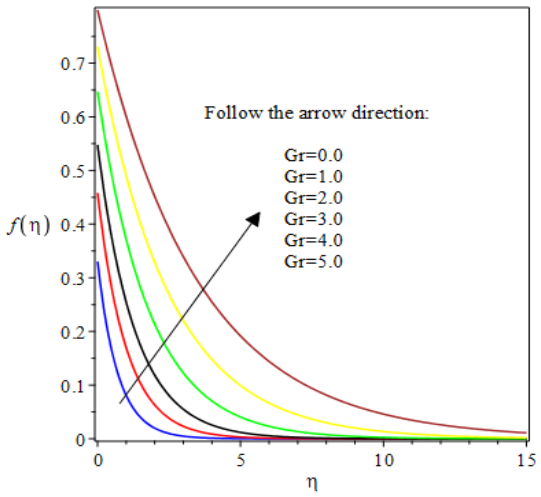

Fig. 12. Effects of Gr on velocity profile

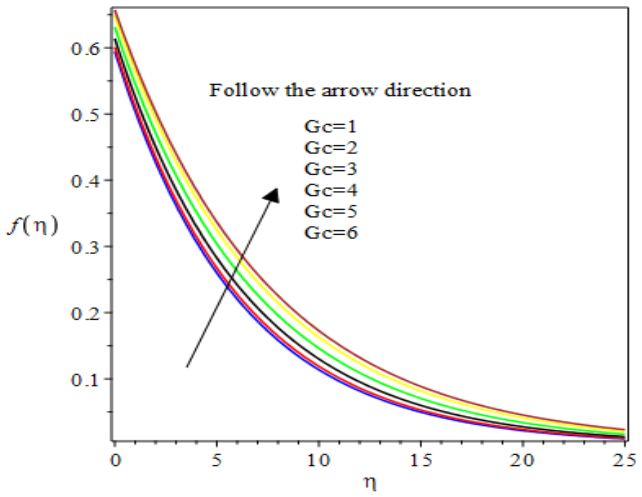

Fig.13. Effects of Gc on velocity profile

Figure 10 shows the effect of suction parameter V_0 .As expected, suction decreases the flow velocity at the surface whereas injection increases it. It is discovered that velocity profile decreases with an increase in the suction parameter due to the fact that momentum boundary layer thickness decreases with a rise in suction velocity. Additionally, the damping effect of suction on the fluid flow can be attributed to the fact that the heated fluid is being pushed towards the plate such that the buoyancy force acted to resist the fluid as a result of high influence of viscosity. Suction velocity on the plate can be used to control boundary layer thickness.

Figure 11 reveals that the velocity decreases with an increase in the magnitude of chemical reaction parameter. The response is due to the fact that the chemical reaction causes an increase in the species concentration boundary layer thickness. In view of this, the concentration buoyancy effect induces chemical reaction increase such that less flow is induced thereby the fluid velocity decreases.

Figures 12 and 13 are plot of velocity fields against η for different values of thermal Grashof number Gr and solutal Grashof numberGc. It is clear from these two figures that the velocity increases as the magnitude of Gr and Gcincreases. From physical point of view, Gr represents the relative effect of the thermal buoyancy force to the viscous hydrodynamic force in the boundary layer. Likewise, Gc defines the ratio of the species buoyancy force to the viscous hydrodynamic force. Thus, the motion of the fluid is accelerated by the enhancement in the buoyancy forces corresponding to an increase in Gr and Gc. As shown in these figures, Gr and Gc have greater impact on the velocity near the plate. The buoyancy force behaves as a favourable pressure gradient accelerating the fluid within the boundary layer.

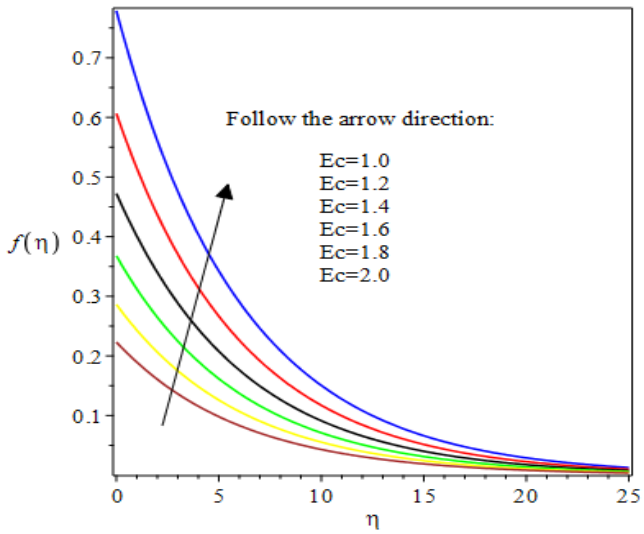

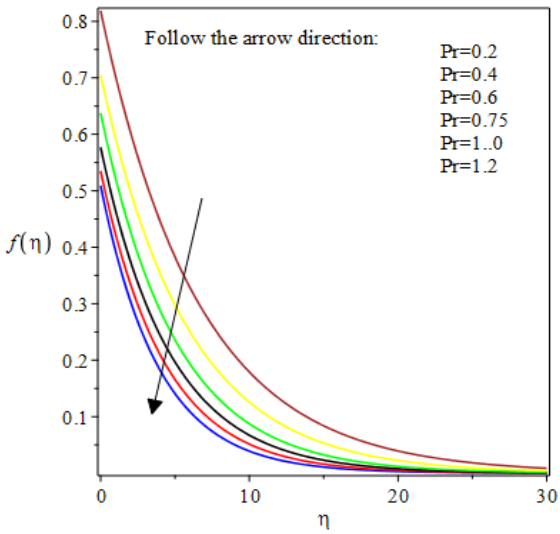

Fig. 14. Effects of Ec on velocity profileFig. 15. Effects of Pr on velocity profile

ISSN No. 2454-6194 | DOI: 10.51584/IJRIAS |Volume VIII Issue XII December 2023

Figure 14 represents the variation of velocity for different value of Eckert number Ec. Eckert number is referred to as fluid motioning controlling parameter. It describes the ratio of kinetic energy of the flow to the boundary layer enthalpy difference; that is, the conversion of kinetic energy into thermal energy by the work done against the viscous fluid stress. An increase in Ec causes the fluid temperature near the plate to rise higher than the plate temperature. This is as a result of the drag between the fluid particles. In consequence, heat is produced. Thus, additional heat will be transferred into the plate and the thermal buoyancy force then increase, causing velocity of the fluid to increase as displayed in the figure 14.

Figure 15illustrates the influence of Prandtl parameters on the velocity distribution across the boundary layer.

Here, observation reveals that the fluid velocity reduces as Prandtl increases. This is due to the fact as the magnitude of Princreases the fluid temperature and its boundary layer thickness diminish. Likewise, the solutal boundary layer thickness falls. In consequence, there is a net reduction in the thermal and solutal buoyancy effects on the momentum equation which results in less induced flow along the plate and thus the fluid velocity decreases. In addition, increase in Pr is an indication of increase in the fluid viscosity, thus as the fluid becomes increasingly viscous the fluid flow is decelerated. The present of Prandtl number retards the velocity profile significantly.

Here, the effects of each of the embedded flow parameters on temperature profile are presented in figures 16-23.Figure 16 shows the effects of thermal Biot number on temperature profile. It is observed that temperature profile increases as the thermal Biot number Bi_1 increases. Conventionally, Bi_1 enhances flow temperature.

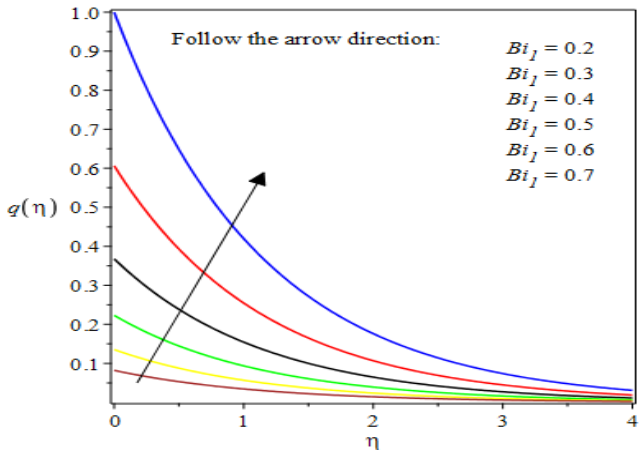

Fig. 16. Effects of Bi_1 on temperature profile

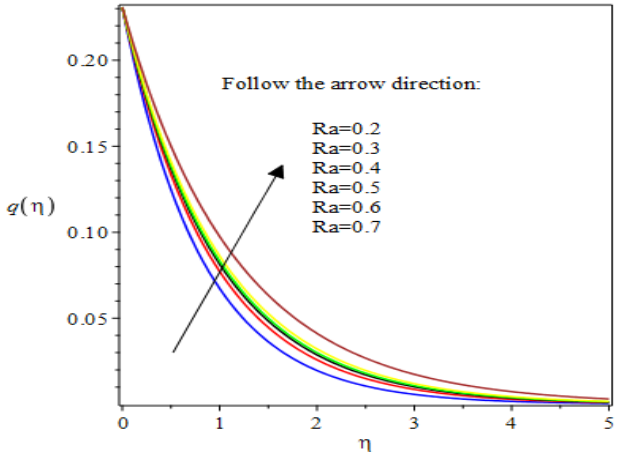

Fig. 17. Effects of Ra on temperature profile

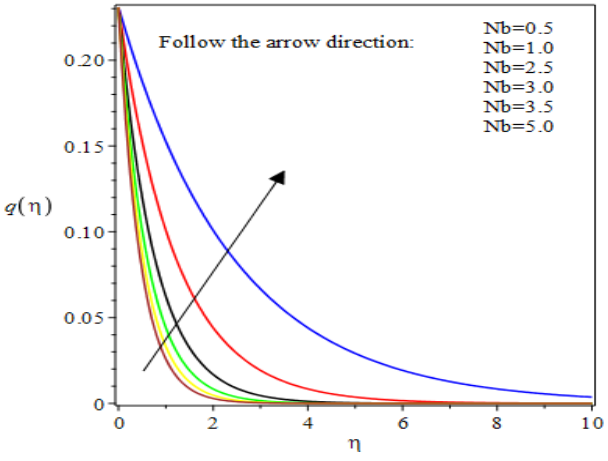

Fig. 18. Effects of Nb on temperature profile

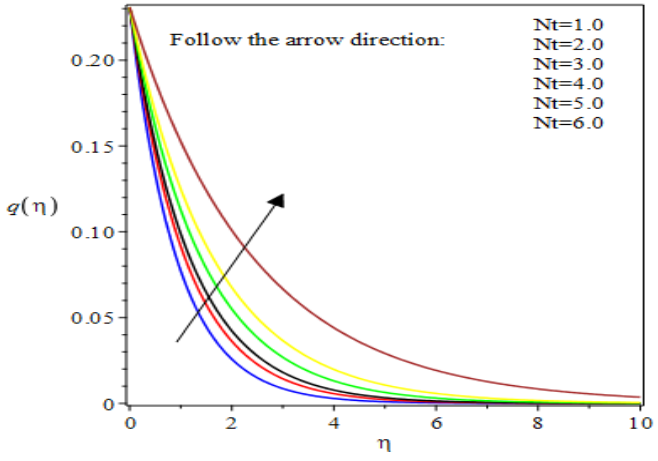

Fig. 19. Effects of Nt on temperature profile

Figure 17 is the sketch of temperature field for a variation in thermal radiation parameter (Ra). Temperature and thermal boundary layer thickness enhance for higher value of thermal radiation parameter Ra. Greater values of Ra yield more heat to the

ISSN No. 2454-6194 | DOI: 10.51584/IJRIAS |Volume VIII Issue XII December 2023

fluid which results in rise in temperature. As we move away from the boundary farther, the Brownian motion parameter makes the velocity decay to zero faster. This is due to the fact that thermal radiation inspires in thickening the thermal boundary layer at the expenses of releasing heat energy from the flow region and it causes the system to cool.In reality this is true because temperature increases as a result of increasing the Rosseland diffusion approximation for radiation.

Figure 18 is the plot for temperature distribution for the impact of Brownian motion parameter Nb. Physically, Brownian motion generates micro-mixing which hikes the thermal conductivity of the fluid. As a results, the temperature increases. Figure 19 shows the effects of increase in thermophoresis parameter on the temperature profile. Thermophoresis Parameter Nt enhances the thickening of thermal boundary layer thickness considerably. In fact, in the presence of thermphoresis the particles are driven towards cold surface from hot surface; hence the temperature and nanoparticle volume fraction increases with rise in thermophoresis

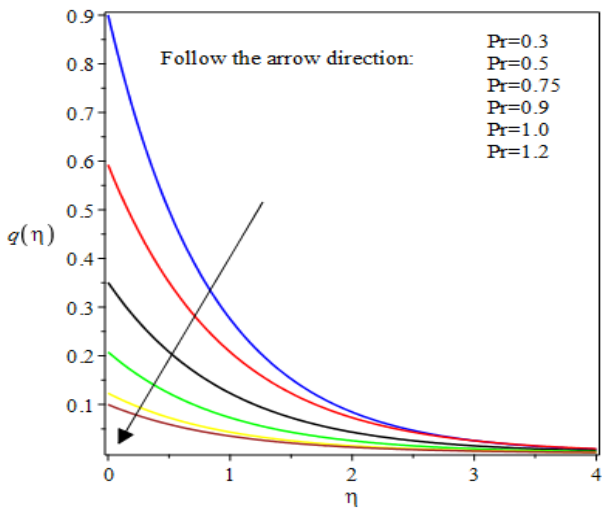

Fig. 20. Effects of Pr on temperature profile

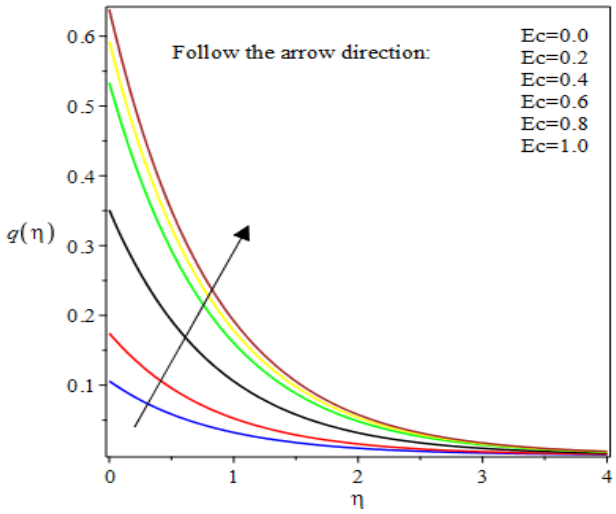

Fig.21. Effects of Ec on temperature profile

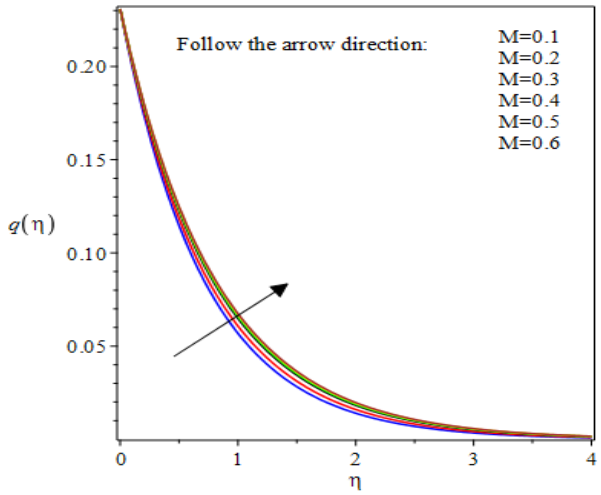

Fig. 22. Effects of M on temperature profile

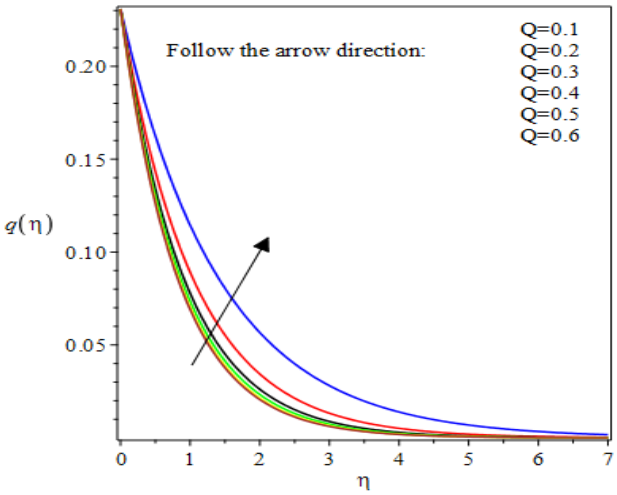

Fig. 23. Effects of Q on temperature profile

The effects of Prandtl number Pr on temperature is shown in Figure 20. This parameter significantly reduces the thermal boundary layer thickness. By definition, Prantle number, is a dimensionless number which is the ratio of momentum diffusivity to thermal diffusivity; that is $\Pr = {\mu C_p}/{k}$. An increase in the values of Prandtl Pr is equivalent to momentum diffusivity which dominates thermal diffusivity. Hence, thermal boundary layer thickness reduces as Pr increases. This is due to the fact the larger the Prandtl number Pr is the higher the viscosity (sticker) of the fluid and the thicker the momentum boundary layer will be compared to the thermal boundary layer. Consequently, heat transfer will be less convective. Figure 21 illustrates the variation of temperature profiles for different values of Eckert number Ec. Observation shows that increasing values of Ec enhances temperature distribution. This response is due to the fact that as Ec increases, heat is generated as a result of the drag between the

ISSN No. 2454-6194 | DOI: 10.51584/IJRIAS |Volume VIII Issue XII December 2023

fluid particles. The internal heat generation inside the fluid increases the bulk fluid temperature which is an indication of additional heating in the flow region due to viscous dissipation. Thus, this additional heat causes increase in the fluid temperature. With an enhancement in value of Eckert number, we see an increase in kinetic energy due to which the temperature is enhanced. Figure 22 illustrates the effects of magnetic parameter M on the temperature. Here, an increase in magnetic parameter leads to an enhancement in the temperature. Physically, larger value of magnetic parameter shows stronger Lorentz force. Such stronger Lorentz force is an agent providing more heat to the fluid due to the fact that higher temperature and thicker thermal boundary layer thickness occur. Thus, the presence of magnetic field in the flow regime decreases the momentum boundary layer thickness and enhances the thermal boundary layer thickness.

Figure 23 shows the effects of the heat source parameter Q on temperature profile. Temperature increases as the heat source parameter increases. This is because heat source releases energy into the thermal boundary layer. Increasing the heat source parameter Q increases the temperature profile and hence it thickens the thermal boundary layer moderately. Here, the effects of each of the embedded flow parameters on concentration profile are presented in figures 24-29

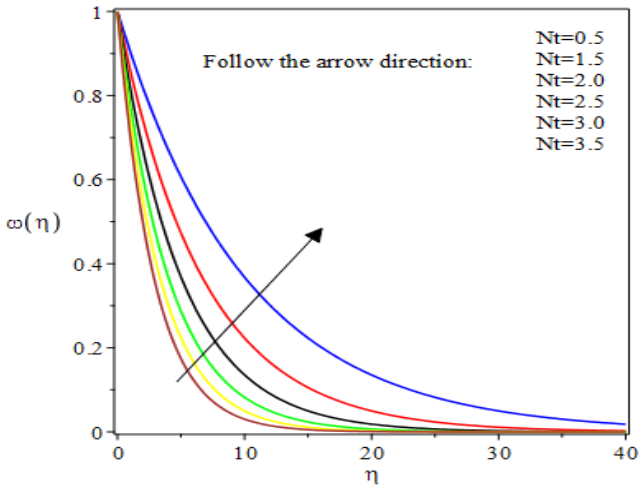

Fig.24. Effects of Nt on concentration profile

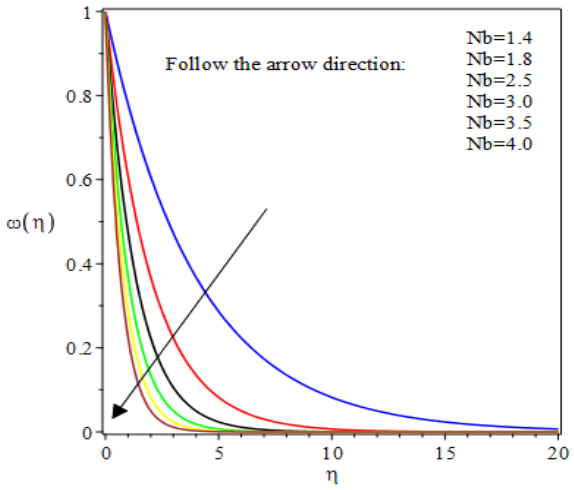

Fig.25. Effects of Nb on concentration profile

Figure 24 shows the effects of thermophoresis parameter Nt on concentration field. It is observed from the figure that the concentration decays monotonically to zero as the distance η increases from the boundary. For large values of Nt, the concentration profile attains its maximum in the boundary layer and then declines to zero faster when go further. Increamement of this parameter enhances the nanoparticles volume fraction strongly. The effects of Brownian motion parameter (Nb) on nanoparticles concentration is shown in Figure 25. As this parameter increases, nanoparticles volume fraction decreases. Higher values of Brownian motion parameter Nb intensifies the nanoparticle collision that results in increment in fluid's temperature and decrement in its concentration. The concentration profile decreases by increasing the Brownian motion p arameter.

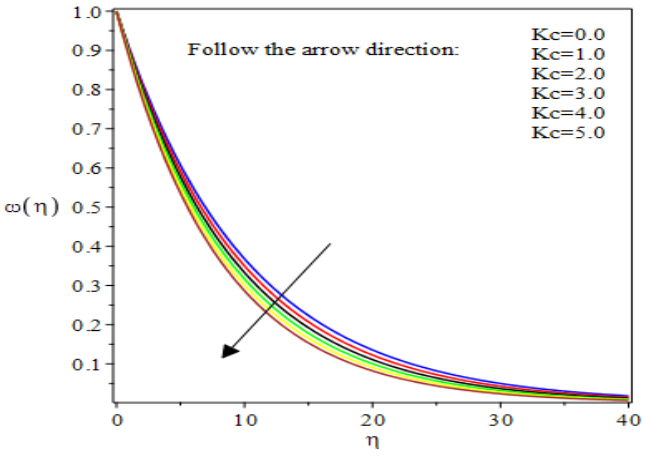

Fig.26. Effects of Kc on concentration profile

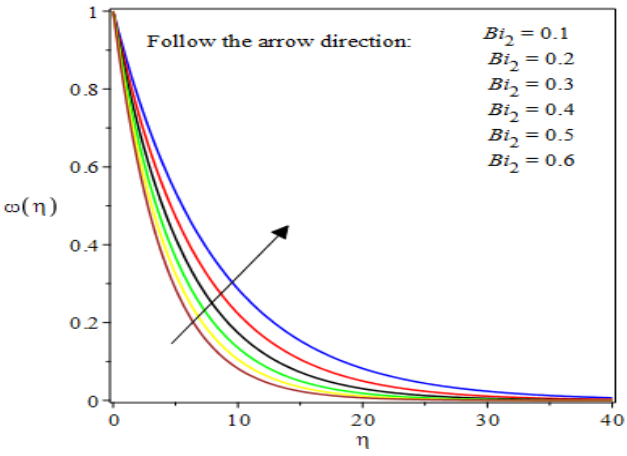

Fig.27. Effect of Bi_2 on concentration profile

ISSN No. 2454-6194 | DOI: 10.51584/IJRIAS |Volume VIII Issue XII December 2023

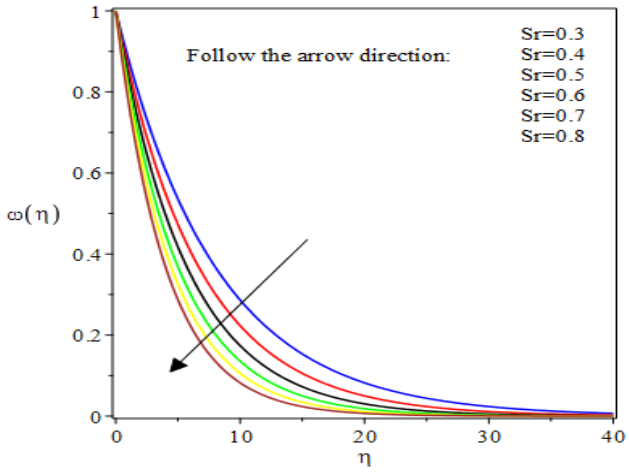

Fig. 28. Effects of Sr on concentration profile

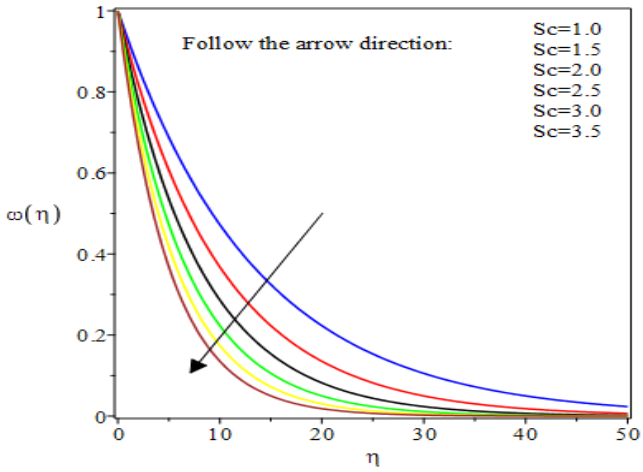

Fig. 29. Effects of Sc on concentration profile

Figure 26 illustrates the influence of chemical reaction parameter Kc on concentration profile. It is observed that an increase in destructive chemical reaction parameter causes a decrease in nanoparticles volume fraction concentration. Figure 27 shows the effects of solutal Biot number on concentration profile. It is observed that concentration profile increases by increasing the solutal Biot number Bi_2.

The effects of Soretnumber Sr on concentration profile is shown in Figure 28. It is observed that increasing in Soret number significantly decreases the nanoparticles volume fraction. Soret number is a dimensionless number which is defined as the ratio of diffusion coefficient and the thermo diffusion coefficient. Soret parameter tends to thicken concentration boundary layer, thus decreasing the mass transfer rate in the wall.

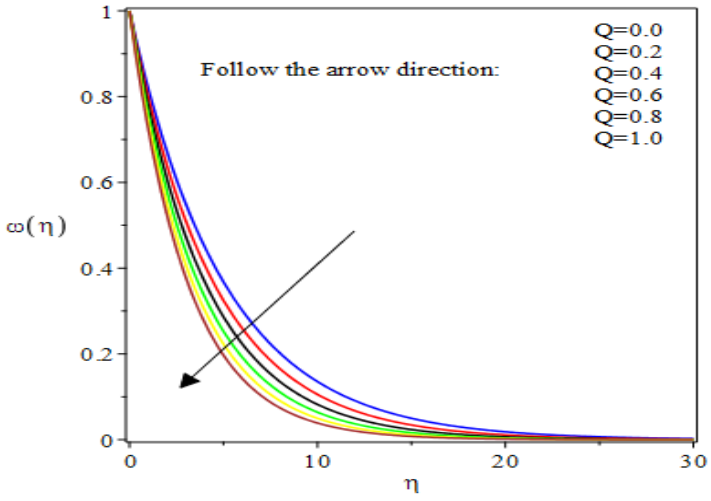

Fig. 30. Effects of Q on concentration profile

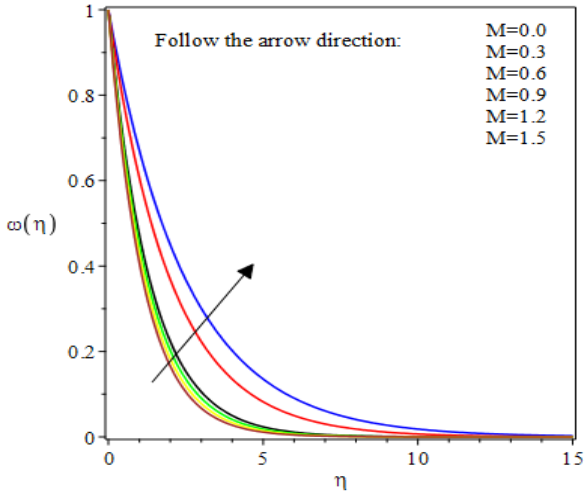

Fig. 31. Effects of M on concentration profile

Figure 29 illustrate the effects of Schimdt number Sc on concentration profile. It is observed that increasing Schimdt number parameter resulted in decreasing in concentration profiles. Schmidt number (Sc) is a dimensionl-ess number defined as the ratio of momentum diffusivity (kinematic viscosity) and mass diffusivity, and is used to characterize fluid flows in which there are simultaneous momentum and mass diffusion convection processes.Large Sc number implies that the molecular diffusivity of the fluid is small and there is concentration decrease. Figure 30 shows the effects of heat source on the nanoparticle concentration. The heat source parameter Q significantly decreases the concentration profile near the boundary layer while the effect of this parameter far from the boundary has almost negligible effect on concentration field.

The effects of magnetic parameter on concentration profile are depicted in Figure 31. Increasing the value of magnetic parameter leads to increase in concentration profile.

ISSN No. 2454-6194 | DOI: 10.51584/IJRIAS |Volume VIII Issue XII December 2023

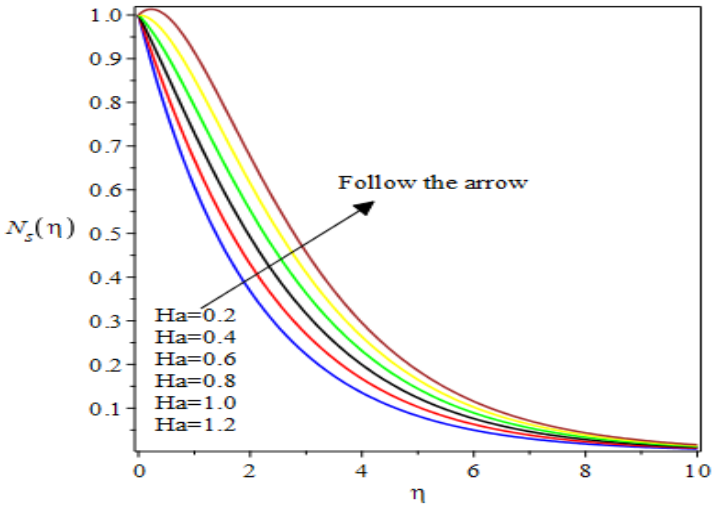

Fig. 32. Effects of Ha on entropy generation profile

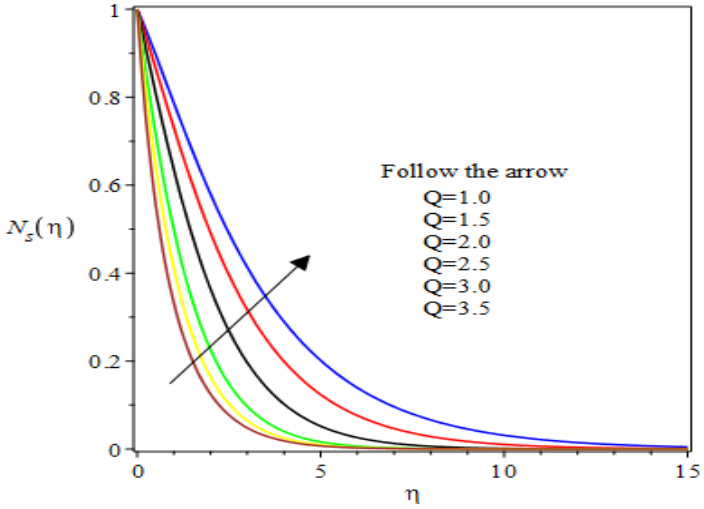

Fig. 33. Effects of Q on entropy generation profile

Effects of each of the embedded flow parameters on entropy generation profile are presented in figures 32-33.Figure 32 illustrates the effect of the Hartmann parameter on the entropy generation number. The entropy generation number is higher for higher Hartmann parameter. The presence of the magnetic field creates higher disorderliness in the fluid thereby increase the entropy generation field. Figure 33 shows the effects of heat generation on entropy generation distribution. The entropy generation number increases as heat supplied to the system increases.

V. Conclusion

This study theoretically investigated magnetohydrodynamic(MHD) flow, entropy generation, heat and mass transfer analysis of unsteady or time dependent fourth grade nanofluid over a vertical plate in a porous medium. The problem is subjected to slip and convective boundary conditions. The formulated system of highly nonlinear coupled partial differential equations (PDEs) governing the problem are transformed to ordinary differential equations (ODEs) using appropriate Lie group similarity variables. Homotopy perturbation Method (HPM) is applied to solve the resulting ODEs. The results obtained through HPM are compared with the published results in the literature as special cases of the present study and found to be in perfect agreement. More so, the obtained HPM results are also verified using numerical method solutions via six order Runge-Kutta integration scheme. Thus, the codes are implemented with the aid of Maplemathematical software package.Bothresults are found to be in excellent agreement at every point (Tables 17).The effects of embedded thermophysical governing flow parameters on dimensionless fourth grade nanofluid flow velocity, temperature, entrop y generation and species concentration distributions across the boundary layer are presented in Tables and graphs and discussed in details. Furthermore, the computation values and impact of some new governing controlling parameters on physical quantities of engineering interest, namely; skin friction coefficient $-f''(0)$, Nusselt number $-q'(0)$, and Sherwood number $-\omega'(0)$ are tabulated and discussed in details. Similar illustration and discussion are also done for the steady fourth grade nanofluid as special case of the present study (unsteady fourth grade nanofluid).

Reference

1. Afridi, M. I., Qasim, M., Khan, I., Shafie, S. and Alshomarani, A. S. (2017). Entropy Generation in Magneto-hydrodynamic Mixed Convection Flow over an Inclined Stretching Sheet. International Journal of Entr-opy, 19 (1), 110. doi:10.3390/e19010010.
2. Akram, S. (2016). Nanofluid effects on peristaltic transport of a fourth grade fluid in the occurrence of inclined magnetic field. ScientiaIranica, 23(3), 1502-1516.
3. Aroloye S. J., Fenuga O. J. and Abiala, I. O. (2017). Unsteady magnetohydrodynamic flow model of a fourth grade fluid in a porous medium. Tran. of Nigeria Association of Mathematical Physics, 5(2017), 263-270.
4. Awan, F. J., Mehmood, A., Mohyud-Din, S. T. and Hassan, S. (2015). On modified algorithm for fourth-grade fluid. Mathematical Problems in Engineering, 10(2015), 1- 6, dio. dio/10.1155/2015/350403.
5. Aziz, T. and Mahomed, F.M. (2012). Close-form solution for a Nonlinear partial differential equation arising in the study of a fourth grade fluid model. Journal of Applied Mathematics, 34(4), 1-16.
6. Aziz,T., Fatima, A. and Mahomed, F. M. (2013). Shock wave solution for nonlinear partial differential equation arising in the study of a non-Newtonian fourth grade fluid model, J. of Applied Mathematics. 22(3),1-5.

ISSN No. 2454-6194 | DOI: 10.51584/IJRIAS |Volume VIII Issue XII December 2023

7. Aziz, T., Magan, A. B. and Mahomed, F. M. (2014). Invariant solution for the magnetohydodynamics (MHD) flow of a fourth grade fluid induced due to the impulsive motion of a flat porous plate. Journal of General and Applied Physics, 7(3), 20-30. doi:10.1007/S13538-014- 0292-9.
8. Bougoffa, L. Duan, J. and Rach, R. (2016). Exact and approximate analytic solutions of the thin film flow of fourth-grade fluids by the modified Adomian decomposition method. International Journal of NumericalMethods for Heat & Fluid Flow, 26(8), 2432-2440.
9. Buongiorno. J. (2006). Convective transport in nanofluids. Journal of Heat Transfer. ASME, 128(1), 240-250.
10. Carim, H. A, Aziz, T. and Mahomed, F. M. (2016). Unsteady MHD flow of a fourth grade fluid caused by an impulsively moving plate in a Darcy porous medium. Int. J. of Modern Physics, 30(3), 145-867.
11. Choi, S. U. S. and Eastma, J. A. (1995). Enhancing thermal conductivity of fluids with nanoparticles. Proceedings of the 1995 ASME International Mechanical Engineering Congress and Exposition, San Francisco, USA.
12. Choi, S. U. S., Zhang, Z. G, Yu, W., Lockwood, F. E. and Grulke, E. A. (2001). Anomalous Thermal ConductivityEnhan cement on Nanotube Suspensions, Applied Physics Letters, 79(14). 2252-2254.
13. Dada, M. S. and Salawu, S. O. (2017). Analysis of heat and mass transfer of an inclined magnetic field pressure driven flow past a permeable plate. Int. J. of Application and Applied Mathematics, 12(1), 189-200.
14. Hayat, T., Mambili-Mamboundou, H. and Mahomed, F. M. (2009). A note on some solutions for the flow of a fourth grade fluid in a porous space. Nonlinear Analysis: Real World Applications, 10(1), 368-374.
15. Hayat, T., Wang, Y. and Hutter, K. (2002). Flow of a fourth grade fluid. Mathematical Models and Methods in Appled Sciences, 12(6), 797–811.
16. Hayat, T., and Naz, R. and Abbasbandy, S. (2011). On flow of a fourth-grade fluid with heat transfer. Int. J. Numer. Meth. Fluids, **67**(4), 2043–2053.
17. He, J. H. (2003). Homotopy Perturbation method: A new non-linear analytical technique, Appl. Maths. 135(1)73-79.
18. He, J. H. (2006).New interpretation of HPM. International Journal of modern Physics B, 20(18), 2561-2568.
19. Hoshyar, H. A., Ganji, D. D. and Abbasi, K. (2015). Analytical solution for porous fin with temperature-dependent heat generation via HPM. Int.J. Appli. Math and Mech. 2(3),15-22.
20. Hussain, T., Shehzad, S. A., Hayat, T. and Alsaedi, A. (2015). Hydromagnetic flow of third grade nanofluid with viscous dissipation and flux conditions. AIP Advances, 5(8), 20-26. dio:1063/1.4929725.
21. Islam, S., Bano, Z., Siddique I. and Siddqui, A. M. (2011). The Optimal solution for the flow of a fourth-grade fluid with partial slip. Computers and Mathematics with Application, 61(6), 1507-1516.
22. Khan, W. A, Culham, J. R. and Makinde O. D. (2015). Combined heat and mass transfer of third grade -grade nanofluids over a convectively heated stretching permeable surface. Can. J. Chem. Eng, 93(3), 1880-1888
23. Nadeem, S., Hayat, T., Abbasbandy, S., and Ali, M. (2010). Effects of partial slip on a fourth-grade fluid with variable viscosity: An analytic solution. Non-Linear Anal: Real World Appl. 11(2),856 -868.
24. Nield, D. A. and Bejan, A. (2006).Convection in Porous Media.(2006). Springer, New York, USA.
25. Pooja Sharma, NavinKumar and Tarun Sharma(2016) Entropy Analysis in MHD Forced Convective Flow through a Circular Channel Filled with Porous Medium in the Presence of Thermal Radiation. International Journal Of Heat And Technology, Vol. 34, No. 2, pp. 311-318
26. Pooja Sharma Tarun Sharma Navin Kumar(2020).Entropy generation analysis of MHD forced convective flow through a horizontal porous channel. Journal Computational and applied research in mechanical Engineering, vol 10(1) page 37 - 49
27. Ramzan, M., Bilal, M., Farooq, U. and Chung, J. D. (2016). Mixed convection radiative flow of second gradenano fluid with convective boundary condition. An optimal solution. Results in Physics, 6(2), 796-804.
28. Sahoo, B., and Poncet, S. (2013). Blasius flow and heat transfer of fourth-grade fluid with slip. Appl. Math. Mech. 34(12), 1465-1480.
29. Shah, R. A., Islam, S. and Siddiqui, A. M. (2010). Couette and Poiseuille flows for fourth grade fluids using optimal homotopy asymptotic method. World Appl. Sci. J., 9(11), 1228–1236.
30. Shehzad, S. A., Hussain, T., Hayat, T, Ramzan, M. and Alsaedi, A. (2015). Boundary layer flow of third grade nanofluid with Newtonian heating and viscous dissipation. J. Cent. South Univ. 22(1), 360-367
31. Tarun Sharma, Pooja Sharma and Navin Kumar (2019). Analysis of Entropy Generation Due to MHD Natural Convective Flow in an Inclined Channel in the Presence of Magnetic Field and Heat Source Effects. BioNano Science Springer. https://doi.org/10.1007/s12668-019-00632-0
32. Tarun Sharma [a], Pooja Sharma [b], Navin Kumar (2023). Chemical reactive magnetized fluid flow through a vertical channel due to heat source and thermal radiation effects, Materials Toady Proceedings Volume 78,Part 3, 2023, Pages 481-492
33. Tarun Sharma, Pooja Sharma, A.H. Seikh, Amjad Iqbal, Navin Kumar(2023).Thermodynamical study of chemically-reactive and thermal-radiative magnetized oscillatory Couette flow in a porous medium filled channel. Case Studies in Thermal Engineering. Volume 48, 103136

ISSN No. 2454-6194 | DOI: 10.51584/IJRIAS |Volume VIII Issue XII December 2023

34. Tarun Sharma Pooja Sharma and Navin Kumar (2021).Entropy generation in thermal radiative oscillatory MHD couette flow in the influence of heat source. J. Phys.: Conf. Ser. 1849 01202
35. Tarun Sharma, Pooja Sharmaand Navin Kumar (2022). Study of dissipative MHD oscillatory unsteady free convective flow in a vertical channel occupied with the porous material in the presence of heat source effect and thermal radiation. J. Phys.: Conf. Ser. **2178** 012012
36. Tarun Sharma, Pooja Sharma, Navin Kumar (2023).Analysis of second law of thermodynamics in unsteady magnetohydrodynamic buoyancy induced flow with heat source and thermal radiation. AIP Conf. Proc. 2768, 020034.Volume 2768, Issue 1, https://doi.org/10.1063/5.0148385
37. Xu, L. (2007). He's homotopy perturbation method for a boundary layer equation in unbounded domain. Computer and mathematics with Applications, 54(7), 1067-1070.
38. Yurusoy, M. (2016). New analytical solutions for the flow of a fourth grade fluid past a porous plate. Journal of Mathematics and Computer Science, 1(2), 29-35.doi:10.11648/j.mcs.20160102.12
39. Zaman, H., Ubaidullah, M., Shah, A. and Ibrahim, M. (2014). Studied the problem of Stokes first problem for an unsteady MHD fourth –grade fluid in a non-porous half space with Hall currents. Journal of Applied Physics, 6(1), 07-14.